Annals of Biomedical Engineering, Vol. 47, No. 8, August 2019 *(© 2019)* pp. 1764–1785
https://doi.org/10.1007/s10439-019-02268-3

Mathematical Modelling and Simulation of Atherosclerosis Formation and Progress: A Review

NIKOLAOS A. AVGERINOS and PANAGIOTIS NEOFYTOU

Thermal Hydraulics and Multiphase Flow Laboratory, National Centre for Scientific Research "Demokritos", Athens, Greece

(Received 14 December 2018; accepted 10 April 2019; published online 24 April 2019)

Associate Editor Dan Elson oversaw the review of this article.

Abstract—Cardiovascular disease (CVD) is a major threat to human health since it is the leading cause of death in western countries. Atherosclerosis is a type of CVD related to hypertension, diabetes, high levels of cholesterol, smoking, oxidative stress, and age. Atherosclerosis primarily occurs in medium and large arteries, such as coronary and the carotid artery and, in particular, at bifurcations and curvatures. Atherosclerosis is compared to an inflammatory disease where a thick, porous material comprising cholesterol fat, saturated sterols, proteins, fatty acids, calcium etc., is covered by an endothelial membrane and a fragile fibrous tissue which makes atheromatic plaque prone to rupture that could lead to the blockage of the artery due to the released plaque material. Despite the great progress achieved, the nature of the disease is not fully understood. This paper reviews the current state of modelling of all levels of atherosclerosis formation and progress and discusses further challenges in atherosclerosis modelling. The objective is to pave a way towards more precise computational tools to predict and eventually reengineer the fate of atherosclerosis.

Keywords—Atherosclerosis, Biochemical, CFD, Haemodynamics, Multiscale multiphysics modelling, LDL mass transport.

THE PATHOPHYSIOLOGY OF ATHEROSCLEROSIS

Atherogenesis is an inflammation-related procedure associated with high concentration of low-density lipoprotein (LDL) in the blood and is affected by systemic risk factors such as hypertension, smoking, hyperlipidemia, hyperhomocysteinemia, and diabetes mellitus.[23] It usually occurs in regions near bifurcations, curves and artery branches where disturbed flow patterns take place and subsequently low values of endothelial shear stress (ESS) are expected.[14] Endothelial cells (ECs) tend to change their morphology when subjected to wall shear stress, i.e. their shape is either elongated under high wall shear stress or rounded/polygonal with no particular alignment pattern under low or oscillating wall shear stress.[85] These conformational changes of ECs associated with low ESS might be responsible for the widening of the junctions between ECs, therefore these small "gaps" between ECs, in combination with flow stagnation and the subsequent prolongation of the residence time of circulating LDL, facilitate the infiltration of LDL underneath the endothelium.[14] The LDL in the artery wall is modified by oxygen radicals to oxidized LDL (oxLDL) causing oxidative stress which in turn induces endothelial cells to express adhesion molecules serving as ligands of leukocytes receptors, such as vascular cell-adhesion molecule-1 (VCAM-1), intercellular adhesion molecule-1 (ICAM-1), and P-selectins[27] subsequently causing the adhesion of blood-borne leukocytes (mainly monocytes and T cells). In addition, oxLDL particles stimulate ECs and smooth muscle cells (SMCs) to secrete monocyte chemotactic protein-1 (MCP-1) and monocyte colony stimulating factor (M-CSF).[103] Once adherent, the leukocyte infiltrates between intact endothelial cells to penetrate into tunica intima. This directed migration requires a chemoattractant gradient: (i) for monocytes it is the particular interaction of MCP-1 that binds to its receptor CCR2 expressed by the monocyte; (ii) for T-cells known chemoattractants include a trio of interferon-γ (IFN-γ)-inducible chemokines of the CXC family that bind to chemokine receptor CXCR3 expressed by T cells.[60]

M-CSF induces entering monocytes to differentiate into macrophages[41] that bind with oxLDL either *via* scavenger receptors (SR) or toll-like receptors (TLR)

Address correspondence to Panagiotis Neofytou, Thermal Hydraulics and Multiphase Flow Laboratory, National Centre for Scientific Research "Demokritos", Athens, Greece. Electronic mail: panosn@ipta.demokritos.gr

expressed on their surface. Binding with SRs internalizes oxLDL and leads progressively to the formation of a foam cell, so named because of the foamy appearance under the microscope, which is the result of the accumulation of lipid droplets within the cytoplasm.[60] During this procedure, internalization and processing of oxLDL induce the presentation of its fragments as antigens on the cell surface and this property of macrophages deems them as antigen-presenting cells (APC). On the other hand binding with TLR can initiate a signal cascade that leads to cell activation by which the activated macrophage produces inflammatory cytokines such as tumour-necrosis factor (TNF), proteases such as matrix metalloproteinases (MMP), and oxygen and nitrogen radical molecules.[40,103] HDL-associated Paraoxonase 1 (PON1) inhibits the influx of cholesterol by oxLDL into macrophages by reducing oxLDL levels, reducing oxLDL uptake *via* the macrophage scavenger receptor and also enhances HDL-mediated cholesterol efflux from the arterial wall into plasma and then to the liver.[27]

T cells in the tunica intima are in search for antigens and undergo activation after interacting with APCs, such as macrophages.[41] The outcome is their differentiation predominantly into T helper 1 (TH1) cells that produce inflammatory cytokines including interferon-γ (IFN-γ) and TNF. These cytokines and others prompt macrophage activation, production of other pro-inflammatory mediators, activate endothelial cells and increase adhesion-molecule expression.[27] In addition, inflammatory cells residing in the plaque, including macrophages, produce angiogenic mediators such as vascular endothelial growth factor (VEGF) promoting neovascularization (Fig. 1).[60]

Thereby the inflammation cycle is maintained, and the atherosclerotic plaque progressively develops. This is formed as (i) the core filled with lipids, including cholesterol crystals, living and apoptotic foam cells and (ii) the fibrous cap consisted of mainly smooth muscle cells and collagen. The mechanism of the formation of the fibrous cap starts with the activation of endothelial cells by oxidative stress and subsequent secretion of platelet-derived growth factor (PDGF) that promotes medial and pre-existing SMCs to migrate near the endothelium. Furthermore, lipid-laden macrophages also secrete PDGF inducing SMC migration through and around them[69] and also basic fibroblast growth factor (FGF) that induces SMC proliferation.[63] In addition, within the developing plaque, the newly developed microvascular vessels may be particularly prone to micro-haemorrhage which leads to thrombin generation triggering platelet release of PDGF, further stimulating SMC migration.[60] Collagen production from SMCs is upregulated by transforming growth factor—beta (TGF-β) which is a pluripotent cytokine secreted by a number of cells, including macrophages, platelets, endothelial cells and SMCs.[41] Interstitial collagen molecules confer most of the tensile strength on the fibrous cap.[60] This continuous process produces a distinct fibrous cap that maintains plaque integrity and avoids contact of the thrombogenic necrotic core with flowing blood.[84] As the plaque becomes more bulky it may protrude into the lumen hampering thereby blood flow consequently leading to ischemia and subsequent clinical manifestations such as angina (Fig. 2).[60]

Plaque vulnerability is promoted by the presence of (i) IFN-γ, which counteracts fibrous cap formation by enhancing collagen degradation and inhibiting smooth muscle cell proliferation and (ii) MMPs that degrade collagen fibers[37] and are, however, counteracted by tissue inhibitors of metalloproteinase (TIMPs) synthesized by ECs, SMCs and macrophages.[88] Therefore, the weakened cap, which cannot withstand the hemodynamic forces may rupture and consequently, expose thrombogenic plaque material (tissue factor) to the blood stream.[41] The subsequent precipitation of platelets and coagulation factors forms a thrombus which if occludes the vessel persistently can lead to an acute myocardial infarction.[60] If the thrombus detaches it may lead to occlusion of important vessels in the circulatory system including cerebral vessels thus leading to a stroke.

MATHEMATICAL MODELLING OF ATHEROSCLEROSIS FORMATION

LDL Mass Transport

Haemodynamics

Blood flow can be either described by the Navier–Stokes (N-S) equation or the modified N-S incorporating Womersley parameter. In the first case Navier–Stokes and the continuity equations of incompressible fluid are:

$$\rho\left(\frac{\partial \boldsymbol{u}}{\partial t} + \boldsymbol{u}\cdot\nabla\boldsymbol{u}\right) = -\nabla p + \mu\nabla^2\boldsymbol{u} \tag{1}$$

$$\nabla\cdot\boldsymbol{u} = 0 \tag{2}$$

where μ is the dynamic viscosity of blood, $\boldsymbol{u}$ is the blood velocity vector in the vessel, ρ is the blood density, and p is the pressure.

In the second case, the general form of the non-dimensional N-S with Womersley parameter is given as[94]:

$$\alpha^2\frac{\partial \boldsymbol{u}}{\partial t} + \mathrm{Re}\boldsymbol{u}\cdot\nabla\boldsymbol{u} + \mathrm{Re}_1\nabla p - \nabla^2\boldsymbol{u} + \frac{R^2}{K}\boldsymbol{u} = 0 \tag{3}$$

where the square root of the oscillatory Reynolds number $a = R(\omega/v)^{1/2}$ is known as Womersley parameter, ω is the circular frequency, R is the inlet radius, Re_1 = max

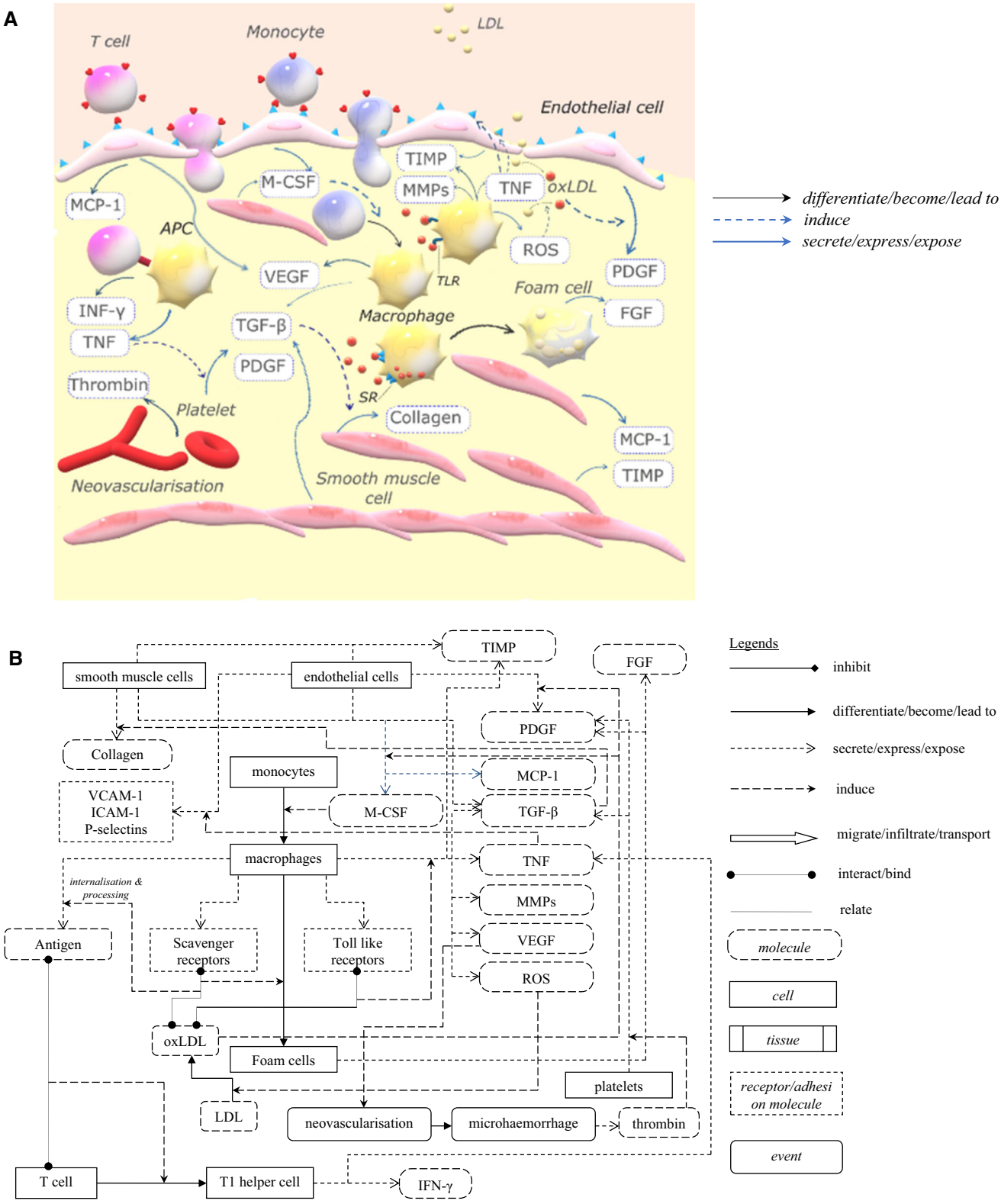

FIGURE 1. (a) Main biochemical interactions of the atherogenesis mechanism. (b) Diagrammatic representation of the main biochemical interactions of the atherogenesis mechanism.

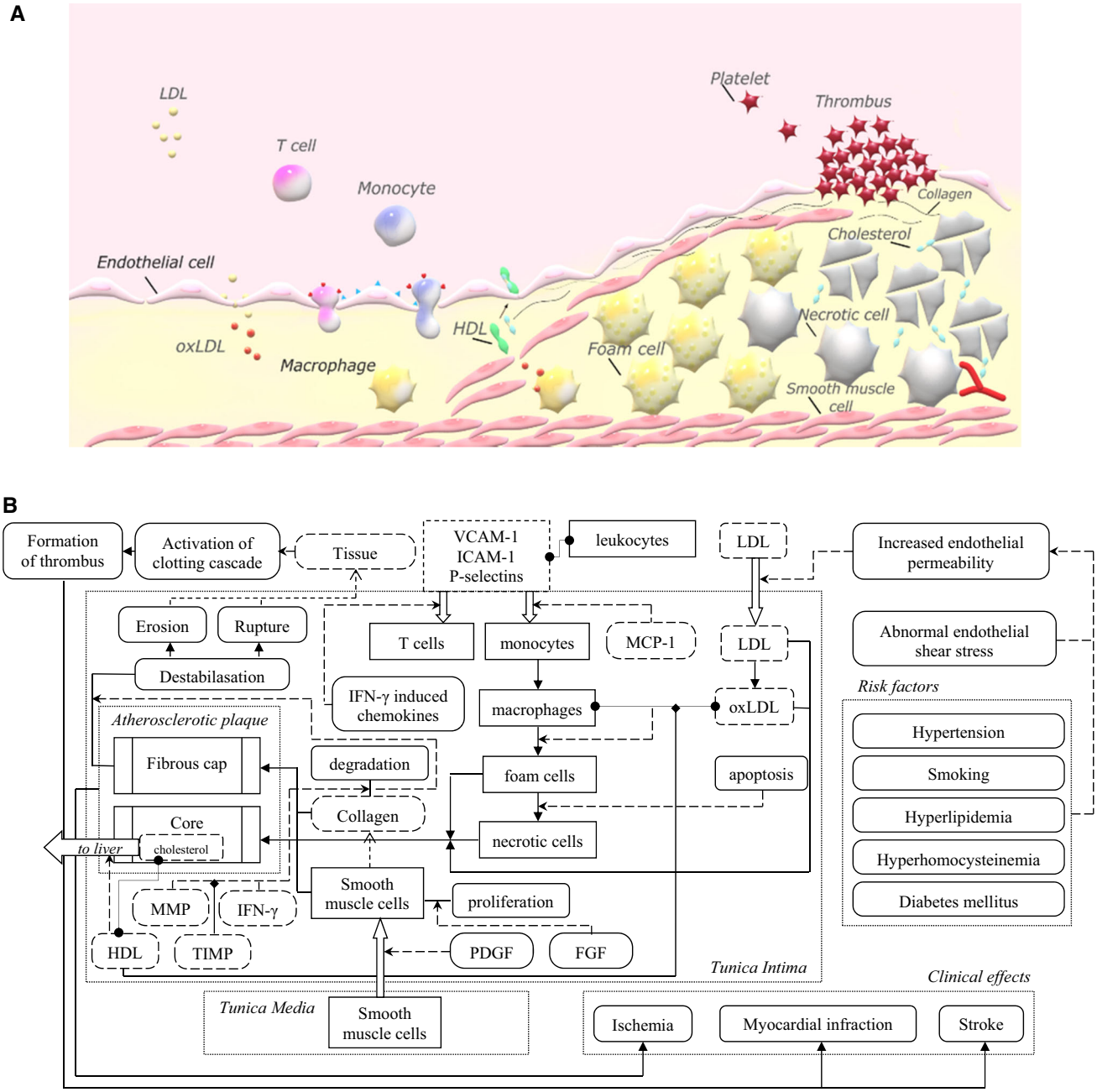

FIGURE 2. (a) Main processes of the atherosclerotic plaque progression and rupture: Entering of Leukocytes into the Tunica Intima and progressive formation of the plaque consisting of the core that the fibrous cap. HDL assists in cholesterol efflux and transport to the liver. (b) Diagrammatic representation of the main processes of the atherosclerotic plaque progression (legends as in Fig. 1b).

{1, Re} and K is the medium Darcian permeability. The Womersley parameter can be interpreted as an estimation of the distance from the artery wall where the viscous forces are of equal magnitude to the inertia. This type of N-S equation addresses time–periodic pressure gradient driving the Poiseuille flow.

Mass transfer of LDL in the blood vessel is coupled with the blood flow N-S equation and is modeled by the general form of the advection–diffusion equation

$$\frac{\partial c}{\partial t} + \nabla \cdot (-D\nabla c + Vc) = 0 \tag{4}$$

where c is the average solute concentration in the blood, and D is the solute diffusivity and the Eulerian approach is followed.

In the case of the modified N-S equation mass transfer in the lumen is described with an advection–diffusion equation with Womersley parameter[94]:

$$\alpha^2 \frac{\partial c}{\partial t} + \mathrm{Re}\boldsymbol{u} \cdot \nabla c - \frac{1}{Sc}\nabla^2 c = 0 \quad (5)$$

where c is the non-dimensional species concentration and Sc is the Schmidt number. An alternative non-dimensionalisation employing the Péclet number (Pe) can be used[26] considering that $Pe = \mathrm{Re}{\cdot}Sc$. Mass in the wall is described by the following non-dimensional equation

$$\alpha^2 \frac{\partial c}{\partial t} + \mathrm{Re}_{\mathrm{eff}}\boldsymbol{u} \cdot \nabla c + \mathrm{Re}_{\mathrm{eff}} Hc - \frac{1}{Sc_{\mathrm{eff}}}\nabla^2 c = 0 \quad (6)$$

Sc_{eff} is the effective Schmidt number given as $Sc_{\mathrm{eff}} = \nu/D_{\mathrm{eff}}$, D_{eff} is the effective diffusivity of species in the wall, $\mathrm{Re}_{\mathrm{eff}}$ is the effective Reynolds number given as $\mathrm{Re}_{\mathrm{eff}} = B^*\mathrm{Re}$ and H is a normalized first order reaction rate for species binding and degradation by the cells of the media and B is a measure of the interactions between the transported species and the wall components.[94]

LDL Infiltration Across the Arterial Wall

The endothelium permeability of the arterial wall is shear stress depended. Due to the blood flow, a frictional force is exerted on the arterial wall, i.e. the wall shear stress (WSS), given by the following equation:

$$\tau_w = \mu \left.\frac{\partial u}{\partial r}\right|_{\mathrm{wall}} \quad (7)$$

where τ_w is the WSS, μ is the dynamic viscosity of the fluid, u is the fluid velocity along the boundary and r is the radial distance from the boundary (the wall). The interconnection between the endothelial transport properties and WSS is expressed by the endothelial cell shape index function (SI), where a portion of the cells will behave as leaky cells (φ) enhancing the endothelium permeability to LDL.[25,99] The amount of LDL and leaky cells determine the transport conditions of the porous model in the lumen.[7,18,70,100] However, in the near-wall region, the WSS also affects the local transport of atherogenic biochemicals from the fluid towards the tissue.[6] In addition, the LDL mass transfer can be affected by the artery movement.[54]

Arterial Tissue as Porous Medium The arterial wall can be treated as a porous medium composed of dispersed cells separated by connective voids where blood flows.[51] The Darcy Law, the Darcy–Forchheimer model, the Brinkman model, the Vafai and Tien, and the Brinkman–Forchheimer–Darcy equation are amongst the transport models that have been proposed to describe the biological phenomena.[50]

The Darcy law represents a linear relationship between the flux and the pressure gradient across the porous medium:

$$q = -\frac{k}{\mu}\nabla p \quad (8)$$

where k is the permeability tensor, q is the flux, μ the dynamic viscosity, and ∇p is the pressure gradient. The fluid velocity u is related to the flux through the porosity φ:

$$u = \frac{q}{\varphi} \quad (9)$$

Darcy–Forchheimer model is a modified model to account for the inertial effects based on a permeability-based Reynolds number and is defined as:

$$\nabla p = -\frac{\mu}{K}V + c_{\mathrm{F}}K^{-1/2}\rho|V|V \quad (10)$$

where c_{F} is a dimensionless parameter related to inertial effects. The permeability-based Reynolds number for the transition to the Darcy–Forchheimer model is defined as:

$$\mathrm{Re}_{\mathrm{K}} = \frac{u_{\mathrm{p}}\sqrt{K}}{\nu} \quad (11)$$

where u_{p}, K, and ν are the pore velocity, permeability, and kinematic viscosity, respectively. Brinkman's model takes into account porous medium solid walls and introduces no-slip boundary conditions and is given by:

$$\nabla p = -\frac{\mu}{K}V + \mu_{\mathrm{e}}\nabla^2 V \quad (12)$$

where μ_{e} is the effective viscosity of the porous medium. In both Darcy and Brinkman transport models the advection–diffusion Eq. (4) can be implemented.

Vafai and Tien[101] proposed a generalized volume averaged model of the expanded Brinkman equation for flow transport through porous media defined as:

$$\frac{\rho_{\mathrm{f}}}{\varepsilon}\left[\frac{\partial V}{\partial t} + \langle (V\cdot\nabla)V\rangle\right] = -\nabla\langle P\rangle^{\mathrm{f}} + \frac{\mu}{\varepsilon}\nabla^2\langle V\rangle - \frac{\mu}{K}\langle V\rangle - \frac{\rho_f F\varepsilon}{K^{1/2}}[\langle V\rangle\cdot\langle V\rangle]J \quad (13)$$

where ε is the medium porosity, F and ρ_{f} are the dimensionless inertia coefficient and the fluid density, respectively. The parameters $\langle P\rangle^{\mathrm{f}}$ and J are the average pressure inside the fluid and a unit vector pointing along the velocity vector V, respectively. The symbol $\langle\ \rangle$, represents the local volume average of a quantity associated with the fluid. In this case species transport is described by the advection–diffusion Eq. (4).

A more detailed model to address transport processes within the arterial layers was proposed by Prosi *et al.*[74]

$$\frac{\partial\langle c\rangle}{\partial t} + \nabla\cdot\left(-D\nabla\langle c\rangle + \frac{\gamma}{\varepsilon}\langle V\rangle\langle c\rangle\right) + k\langle c\rangle = 0 \quad (14)$$

where γ is the hindrance coefficient for the transport of species and k is the reaction rate constant.

Finally, an extensive model to describe LDL transport in each arterial layer namely the endothelium, intima, IEL and media, comprises of the following set of volume-averaged equations for the fluid flow and the species transportation was employed for the endothelium and IEL:

$$\frac{\rho}{\varepsilon}\frac{\partial\langle V\rangle}{\partial t}+\frac{\mu}{K}\langle V\rangle=-\nabla\langle p\rangle^{\mathrm{f}}+R_u T\sigma_{\mathrm{d}}\nabla c+\mu'\nabla^2\langle V\rangle \quad (15)$$

$$\frac{\partial\langle c\rangle}{\partial t}+\left(1-\sigma_f\right)\langle V\rangle\cdot\nabla\langle c\rangle=D_c\nabla^2\langle c\rangle \quad (16)$$

and for the intima and media layers

$$\frac{\rho}{\varepsilon}\frac{\partial V}{\partial t}+\frac{\mu}{K}V=-\nabla p^{\mathrm{f}}+\mu'\nabla^2 V \quad (17)$$

$$\frac{\partial\langle c\rangle}{\partial t}+\left(1-\sigma_f\right)\langle V\rangle\cdot\nabla\langle c\rangle=D_c\nabla^2\langle c\rangle+k\langle c\rangle \quad (18)$$

where μ' the effective dynamic viscosity, σ_{f} is the Staverman filtration reflection coefficient, σ_{d} is the Staverman osmotic reflection coefficient, T is the absolute temperature, and R_{u} is the universal gas constant. It can be seen that for the IEL and endothelium the Staverman filtration and osmotic reflection coefficients, associated to the permeability of the membranes to solutes such as LDL, are incorporated in the corresponding equations.[104]

Arterial Tissue as Membrane In order to resolve the cell membrane permeability characteristics, correlations for the transmural velocity (J_{v}) and the solute flux (J_{s}) at the lumen–wall interface are used. These are the Kedem-Katchalsky (K–K) equations given by

$$J_{\mathrm{v}}=L_{\mathrm{p}}(\Delta p-\sigma\Delta\pi) \quad (19)$$

$$J_{\mathrm{s}}=\omega\Delta\pi+(1-\sigma)J_{\mathrm{v}}\bar{c} \quad (20)$$

where L_{p} is the hydraulic permeability, Δp is the pressure difference and $\Delta\pi$ is the osmotic pressure difference between the semipermeable membrane sides, ω is the solute permeability coefficient, σ is the reflection coefficient and $\bar{c}$ is the mean solute concentration of endothelium.[48]

Another expression of the K–K equations to describe the flux across the endothelium and IEL incorporates the Staverman reflection coefficients and is given by[47]:

$$J_{\mathrm{v}}=L_{\mathrm{p}}(\Delta p-\sigma_{\mathrm{d}}\Delta\pi) \quad (21)$$

$$J_{\mathrm{s}}=P\Delta c+\left(1-\sigma_f\right)J_{\mathrm{v}}\bar{c} \quad (22)$$

The permeability coefficient of the wall layer is P whereas Δc is the osmotic concentration difference. The Staverman osmotic reflection coefficient σ_{d} denotes the ability of as solute to induce osmotic flow in the sense that if a membrane can have pores so small as to completely exclude the solute or so large that the solute completely passes through then the full ($\sigma_{\mathrm{d}}=1$) or null ($\sigma_{\mathrm{d}}=0$) osmotic potential respectively is realized. The Staverman filtration reflection coefficient σ_{f}, denotes the ability of a membrane to sieve a solute in a filtration in the sense that $\sigma_{\mathrm{f}}=1$ if the solute is completely excluded and $\sigma_{\mathrm{f}}=0$ if the membrane is unselective.[10] Albeit some studies consider σ_{d} and σ_{f} as equal[3,49,104] others suggest non-equal values for σ_{d} and σ_{f} for both the endothelium and IEL.[46] In addition to the latter, Shu *et al*[87] argue that the assumption that coefficients σ_{d} and σ_{f} in the classical K–K equations are equal cannot be valid for osmosis in the nanoscale. Therefore, they propose a modified version incorporating three new parameters, namely the osmotic pressure coefficient (σ_{o}), the primary filtration coefficient (σ_{s}) and the secondary selectivity rate (x), instead of the two coefficients, that is given by

$$J_{\mathrm{v}}=L_{\mathrm{p}}(\Delta P-\sigma_{\mathrm{o}}\pi) \quad (23)$$

$$J_{\mathrm{s}}=\omega L_{\mathrm{p}}\Delta\pi+x(1-\sigma_s)cJ_{\mathrm{v}} \quad (24)$$

Thereby Eqs. (23) and (24) are able to accurately take into account the osmosis through nano-pores.

Traditional Kedem–Katchalsky membrane equations have two major disadvantages. First, a steady-state condition is considered in the endothelium and the IEL. Second, the boundary effects on the flow across the membrane are ignored, which is not valid when the boundaries of the porous membrane have to be accounted for.[50] For this reason a modified version of Kedem–Ketchalsky's equations for the solute flux through the endothelium has been presented:

$$J_{\mathrm{s}}=P\left(c_{\mathrm{lum}}-c_{\mathrm{w,end}}\right)\frac{P_{\mathrm{e}}}{e^{\mathrm{Pe}}-1}+J_{\mathrm{v}}(1-\sigma)c_{\mathrm{lum}} \quad (25)$$

$$\mathrm{Pe}=\frac{J_{\mathrm{v}}(1-\sigma)}{P_{\mathrm{i}}} \quad (26)$$

where P is the diffusive permeability, Pe is the modified Péclet number, $c_{\mathrm{w,\ end}}$ the LDL concentration in the arterial wall at the sub-endothelial layer, and σ is the solvent drag coefficient.[73]

The flux of fluid and solutes within biological membranes considering osmotic pressure and active transport mechanisms and the alteration of their ionic distribution due to their charges has been described by an enhanced K–K set of equations as:

$$J_v = L_p\left(\Delta P - \sum\nolimits_k \left(\sigma_k RT\Delta C_k - (1-\sigma_k) z_k F\overline{C}_k \Delta\varphi\right)\right) \quad (27)$$

$$J_i = (1-\sigma_i) J_v \overline{C}_i + \omega_i\left(RT\Delta C_i + z_i \overline{C}_i F\Delta\varphi\right) \quad (28)$$

where z_k is the charge number of species k, F is the Farraday constant and $\Delta\varphi$ is electrical potential difference, whereas summation denotes a variety of solutes.[17] The enhanced K–K equations can fill the gap of the traditional version of K–K theory regarding the recovery of the Donnan equilibrium where fixed charges induce imbalance of ionic concentrations and develop an osmotic pressure gradient between the inside and outside environments of the membrane. An additional term J_{ai} can be added at the RHS of Eq. (28) accounting for the active ionic transport. The work of Cheng and Pinsky[17] is a step forward compared to previous studies of Li[56] that incorporated the electrostatic potential difference between solutes, yet not able to address the Donnan equilibrium or the work of Hodson and Earlam[43] using the K–K theory with fixed charges but only for binary solutions and not for active transport.

Fluid-Wall Models and Boundary Conditions In general, numerical models of LDL mass transfer in the arterial wall have been classified into three distinct types, i.e. the wall free model, the fluid-wall single layer model and the fluid-wall multilayer model.[74] The pertinent boundary conditions for fluid and solute for the different arterial transport models are described as follows.

In the wall free model, the solution of the blood flow in the lumen is independent of the mass transport mechanism within the artery wall, thus only considering the necessary boundary conditions, i.e. for instance filtration velocity value from the literature, for the wall effect. In this sense the wall-free model does not address solute concentration within the wall. For the wall-free model at the flow entrance a constant filtration velocity is prescribed and for the solute diffusive flux is used at the wall.[76]

The homogenous wall model is the first to address LDL transport to the arterial wall. For the homogenous wall model at the lumen inlet and outlet an "insulation" condition is used. A lumen to wall transmural velocity in the normal direction of the endothelium wall side is used. At the media-adventitia interface a pressure condition was assumed. For the solute convection–diffusion equation constant concentration and a convective flux condition were assumed at the lumen inlet and outlet. At the wall side of the endothelium a flux in the normal direction is used. Finally, a constant concentration is used at the media-adventitia interface.[96]

The fluid-wall multi-layer model is a very comprehensive model incorporating the wall heterogeneity considering distinctively the different properties of each arterial layer either as a membrane or as a porous medium.[50] A version of this model is the four-layer model[104] where the endothelium, intima, internal elastic lamina (IEL) and media are all treated as macroscopically homogeneous porous media employing Eqs. (15)–(18). The solid boundaries effects of the different porous layers are neglected. The hydraulic pressure at the lumen-endothelium and the media-adventitia interfaces are 100 mmHg. The reference filtration velocity is taken as 2.31×10^{-5} mm·s^{-1}. Continuity of velocity is applied at the lumen-endothelium-intima-IEL-media interfaces. For the solute concentration a total mass flux boundary condition is applied at the endothelium-intima-IEL-media interfaces. At the lumen-endothelium interface net transmural flux is used. Between the media and adventitia, the boundary condition applied is $\partial c/\partial n = 0$. In the work of Yang and Vafai[105] analytical solutions for LDL transport in the arterial wall are presented but their use is limited to straight geometry.

The basic layers of the artery wall are shown in Fig. 3, whereas the pertinent mass transfer models and the corresponding boundary conditions are summarized in Tables 1 and 2 respectively.

Atherosclerosis Inflammatory Processes

LDL Oxidation and the Role of HDL

Oxidation of LDL was first modelled by Stanbro[93] using an ordinary differential equation (ODE) and later on Cobbold *et al.*[20] proposed a system of time-

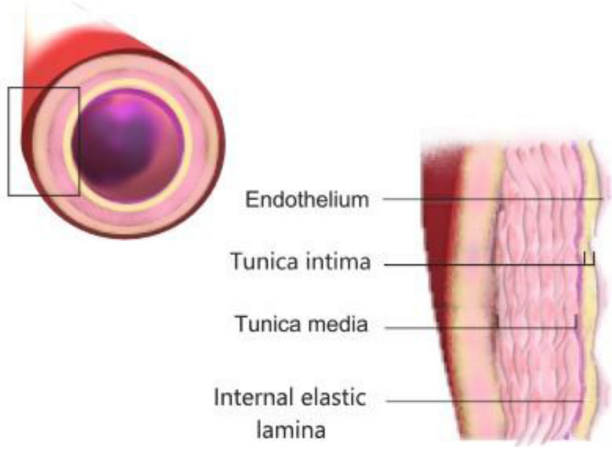

FIGURE 3. Arterial wall cross-section. Widths of layers pertinent to modelling are Endothelium—2 μm, Tunica intima—10 μm, IEL—2 μm, Tunica media—200 μm.[49]

TABLE 1. Summary of mass transfer models of fluid and solute in the lumen and the arterial wall.

	Lumen		Wall			
			Porous media		Membrane	
	Reference	Equations	Reference	Equation	Reference	Equation
Fluid	Stangeby and Ethier[94] Khakpour and Vafai[50]	(1)–(3)	Khakpour and Vafai[50]	(8), (10), (12)	Kedem and Katchalsky[48]	(19)
			Vafai and Tien[101]	(13)	Shu *et al.*[87]	(23)
			Yang and Vafai[104]	(15), (17)	Cheng and Pinsky[17]	(27)
Solute		(4), (5)	Stangeby and Ethier[94]	(6)	Kedem and Katchalsky[48]	(20)
			Prosi *et al.*[74]	(14)	Shu *et al.*[87]	(24)
			Yang and Vafai[104]	(16), (18)	Patlak *et al.*[73]	(25)
					Cheng and Pinsky[17]	(28)

dependent ODEs based on *in vitro* experimental data. A second order kinetic reaction was used to model the interaction between LDL and free radicals. Calvez and Ebde[12] proposed an improved version of this approach to describe the evolution of the oxLDL (Ox) concentration and the subsequent transformation of macrophages into foam cells. In their PDE the second term at the left-hand side represents the lesion growth indicating that the Ox molecules are transported along with the tissue deformation having velocity u. The same model was used by Silva *et al.*[89] A similar approach was frequently used, where synthesis and turnover of oxLDL were modelled as a reaction with radicals.[12,19,32,34,36,42,78,89] On the other hand, a simplified approach was proposed by Cohen *et al.*[21] considering LDL oxidation as a constant. The works of Friedman and Hao[34] and Hao and Friedman[42] expanded the original model and incorporated the impact of the HDL concentration. In their analysis HDL reacts with free radicals and oxidates. Table 3 summarises the governing equations used in LDL oxidation.

MCP-1 Secretion

The response of the endothelial cells in the presence of ox-LDL is the secretion of MCP-1 that initiates the monocytes recruitment into the intima.

Hao and Friedman[42] included MCP-1 production by the endothelial cells assuming a constant concentration.[79] Production, diffusion and degradation rate of MCP-1 were set according to Chen *et al.*[15] In the work of Mckay *et al.*[64] the evolution of monocytes concentration was modeled using a differential equation considering the effect of chemo-attractants and the subsequent proliferation and the formation of macrophages. Monocytes production rate, maturing rate into macrophages, and the proliferation rate were necessary parameters for the modelling. In the model of Cilla *et al.*[19] a diffusion-convection differential equation was used incorporating production and degradation of MCP-1. In their study diffusion and convection terms were disregarded. Cytokines production and degradation rates were set according to Siogkas *et al.*[90] and Zhao *et al.*,[109] and the threshold of LDL and monocytes mitosis as in Schwenke and Carew.[83] In other studies, the secretion of MCP-1 was grouped together with other chemoattractants such as interleukin-1 (IL-1) and M-CSF.[31,45,64,89,108] A summary of the governing equations used in the secretion of monocyte chemoattractant protein is presented in Table 4.

Monocyte Recruitment

The existence of monocytes in the lumen has rarely been considered. Cilla *et al.*[19] presented monocyte dispersion process along the lumen and in the intima. Similar approaches for the monocyte diffusion in the wall have also been proposed.[11,64] Chalmers *et al.*[13] included monocyte chemoattractant flux into the intima. Monocyte production in the endothelial cells was determined as a function of cytokine and modified LDL concentration. The transport of monocytes through the intima-media domain has been modeled as a purely diffusion–reaction equation. In other studies a system of reaction–diffusion PDEs describing the density of immune cells (monocytes, macrophages) and the density of the cytokines secreted by the immune cells has been proposed.[52,53] In other studies, the monocyte recruitment and differentiation has been simplified and incorporated into the governing equation of the macrophage density describing the conversion of macrophages into foam cells after reaction with oxLDL.[12,32,89,99] Monocytes concentration in the intima could be either incorporated as a constant value[32] or a function of a pro-inflammatory signal S.[89] The governing equations used in monocyte recruitment are summarized in Table 5.

TABLE 2. Boundary conditions for mass transfer models of the arterial wall with *u*, *p* and *c* the fluid velocity, pressure and LDL concentration respectively.

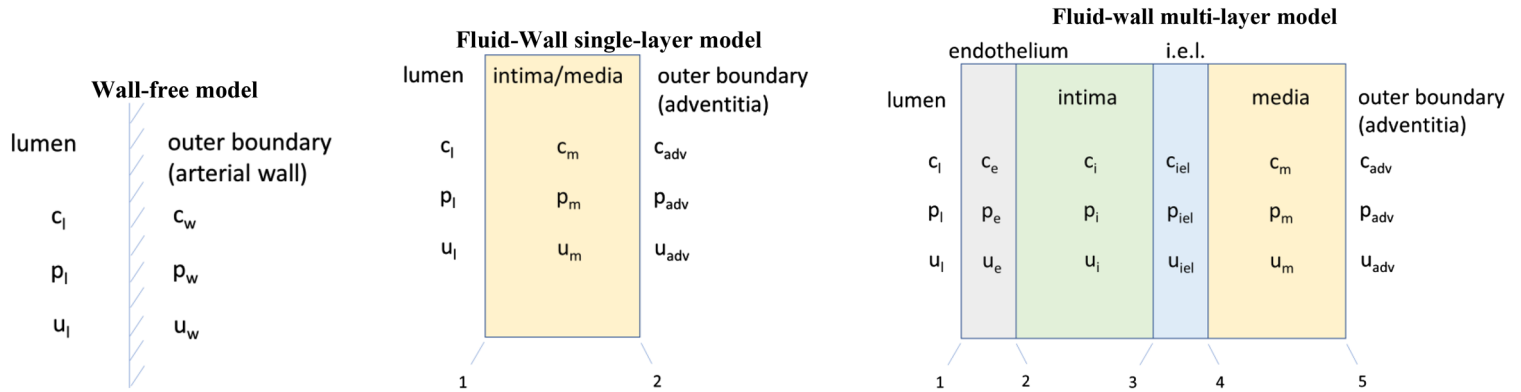

Boundary conditions

Fluid	Interface[28,68,75]	$u_{filt} = \text{const}$	Interface 1[70,81,94,96]	$n_w \cdot u_w = -J_v$	Interface 1[105]	p = 100 mmHg, $\frac{\partial u_{filt}}{\partial n} = 0$
					Interface 2–4[105]	$\frac{\partial u_{filt}}{\partial n} = 0$
			Interface 2[70,81,94,96]	$p_w = p_{adv}$, $\frac{\partial u}{\partial n} = 0$	Interface 5[102,104,105]	p = 30mmHg, $\frac{\partial u_{filt}}{\partial n} = 0$
Solute	Interface[28,68,75]	$q_w = -D\frac{\partial c}{\partial n} = \alpha c_w$	Interface 1[70,81,94,96]	$(-D_l \nabla c_l + \boldsymbol{u}_l c_l) \cdot \boldsymbol{n}_l = J_s$	Interface 1-4[102,104,105]	$\left[(1-\sigma_f)V_c - D_e\frac{\partial c}{\partial n}\right]_+ = \left[(1-\sigma_f)V_c - D_e\frac{\partial c}{\partial n}\right]_-$
				$(-D_w \nabla c_w + u_w c_w) \cdot n_w = J_s$		
			Interface 2[70,81,94,96]	$\partial c/\partial n = 0$	Interface 5[102,104,105]	$c/C_o = 0$ or $c/C_o = 0.01$ or $\partial c/\partial n = 0$

TABLE 3. Summary of the governing equations used in LDL oxidation.

Reference	Governing equations			
Calvez and Ebde,[12] Silva *et al*[89]	$\begin{cases} \partial_t Ox + div(uOx) = d_1 \Delta Ox - k_1 Ox \cdot M, & \text{for all}(x,y) \\ \partial_y Ox = \tau(x) C, & \text{if} y = h \\ \partial_y Ox = 0, & \text{if} y = 0 \end{cases}$			
	Ox:	Ox-LDL concentration	M:	Macrophages concentration
	d_1:	10^{-3} cm^2·s^{-1}	C:	LDL concentration
	k_1:	1 cm·g^{-1}·s^{-1}	$\tau(x)$:	Blood vessel permeability
Gessaghi *et al*.[36]	$\dot{m}_{ox} = km$			
	$\dot{m}_{ox}$	LDL oxidation rate per unit area	m:	Intimal LDL mass accumulation per unit surface area
	k	Oxidation rate		
Reddy and Seshaiyer[78]	$\frac{\partial L}{\partial t} = D_L \nabla^2 L - k_L LM + L_0$			
	L:	LDL/ox-LDL concentration rate	M:	Macrophages concentration rate
	D_L:	LDL/ox-LDL diffusion coefficient	L_o:	LDL molecule input
	k_L:	LDL/ox-LDL reaction rate		
Cilla *et al*.[19]	$\frac{\partial C_{LDL,w}}{\partial t} + \nabla \cdot \left(-D_{LDL,w} \nabla C_{LDL,w}\right) + u_w \cdot \nabla C_{LDL,w} = -d_{LDL} C_{LDL,w} - LDL_{oxr} C_{LDL_{ox},w} C_{M,w}$			
	$C_{LDL,w}$:	Ox-LDL concentration	d_{LDL}:	LDL degradation rate
	$D_{LDL,w}$:	Ox-LDL diffusion coefficient	LDL_{oxr}:	LDL uptake rate by macrophage
	u_w:	Transmural velocity vector field	$C_{M,w}$:	Macrophages concentration
Hao and Friedman[42]	$\begin{cases} \frac{\partial L}{\partial t} - D_L \Delta L = -k_L rL \\ \frac{\partial H}{\partial t} - D_H \Delta H = -k_H rHG \\ \frac{\partial L_{ox}}{\partial t} - D_{L_{ox}} \Delta L_{ox} = k_L rL - \lambda_{L_{ox}M} ML_{ox} \end{cases}$			
	L:	LDL concentration	k_H:	HDL oxidization rate
	D_L:	LDL diffusion coefficient	G:	PDGF concentration
	k_L:	LDL oxidization rate	L_{ox}:	Ox-LDL distribution rate
	r:	Free radicals concentration	D_{Lox}:	Ox-LDL diffusion coefficient
	L:	LDL distribution	λ_{LoxM}:	Ox-LDL reduction rate
	H:	HDL distribution	M:	Macrophages density
	D_H:	HDL diffusion coefficient		
Friedman and Hao[34]	$\frac{\partial H}{\partial t} - D_H \Delta H = -k_H rH - \frac{k_{AF}}{1+m} \frac{HF}{K_F + F}$ $\frac{\partial L_{ox}}{\partial t} - D_{L_{ox}} \Delta L_{ox} = k_L rL - \lambda_{L_{ox}M_1} \frac{L_{ox}}{K_{L_{ox}} + L_{ox}} M_1 - \lambda_{L_{ox}M_2} \frac{L_{ox}}{K_{L_{ox}} + L_{ox}} M_2$			
	H:	HDL concentration	L_{ox}:	Concentration of ox-LDL
	D_H:	HDL diffusion coefficient	D_{Lox}:	Diffusion coefficient of oxidized LDL
	k_H:	Reaction rate of HDL with radical	K_{Lox}:	ox-LDL saturation for production of MCP-1
	r:	Free radicals concentration	λ_{LoxM2}:	Rate of ox-LDL ingestion by M2 Macrophages
	k_{AF}:	Reaction rate of HDL removing ox-LDL from foam cells	M_1:	M1 macrophages density
	F:	Foam cells density	M_2:	M2 macrophages density
	K_F:	Foam cells saturation		

TABLE 4. Summary of the governing equations used in the secretion of monocyte chemoattractant protein.

Reference	Governing equations		
Hao and Friedman[42]	$\frac{\partial P}{\partial t} - D_P \Delta P = \lambda_{PE} \frac{L_{ox}}{K_{Lox} + L_{ox}} - d_P P$		
	P: MCP-1 concentration	L_{ox}:	ox-LDL distribution
	D_P: MCP-1diffusion coefficient	K_{Lox}:	ox-LDL saturation for production of MCP-1
	λ_{PE}: MCP-1 production rate		
Mckay *et al.*[64]	$\frac{dC}{dt} = \rho_C L_{ox} - d_C C$		
	C: Chemo-attractant density	L_{ox}:	ox-LDL density
	ρ_C: Chemo-attractant production due to ox-LDL	d_C:	Chemo-attractant degradation
Cilla *et al.*[19]	$\frac{\partial C_{c,w}}{\partial t} = -d_c C_{c,w} + C_r C_{LDL_{ox,w}} C_{m,w}$		
	$C_{c,w}$: Cytokines concentration	$C_{LDL_{ox,w}}$:	Ox-LDL concentration
	d_c: Cytokines degradation rate	$C_{m,w}$:	Monocytes concentration
	C_r: Cytokines production rate		
Filipovic *et al.*[31]	$\partial_t S = d_3 \Delta S - \lambda S + k_1 Ox \cdot M + \gamma(Ox - Ox^{thr})$		
	S: Cytokines concentration	Ox:	Ox-LDL
	d_3: Diffusion coefficient	M:	Macrophages concentration
	λ: Degradation coefficient	γ:	Ox-LDL detection coefficient
	k_1: Solute lag coefficient		

TABLE 5. Summary of the governing equations used in monocyte recruitment.

Reference	ions		
Cilla *et al.*[19]	Lumen		
	$\nabla \cdot (-D_{m,l} \nabla C_{m,l}) + \boldsymbol{u}_1 \cdot \nabla C_{m,l} = 0$		
	D_m: monocyte diffusion coefficient in the lumen	$C_{m,l}$: monocyte concentration in the lumen	
Cilla *et al.*[19]	Wall		
	$\frac{\partial C_{m,w}}{\partial t} + \nabla \cdot (-D_{m,w} \nabla C_{m,w}) + = -d_m C_{m,w} - m_d C_{m,w} + C_{m,w} C_{LDL_{ox},w} exp \frac{-C_{m,w}^2}{2C_{m,w^2}^{th}}$		
	$C_{m,w}$: Monocytes concentration	$C_{LDL_{ox},w}$:	Ox-LDL
	d_m: Monocytes differentiation rate	C_{m,w^2}^{th}:	Monocytes mitosis threshold
	m_d: Monocytes natural death		
Bulelzai and Dubbeldam[11]	$\frac{dm}{dt} = (\Gamma(\sigma_w, L_{ox}) - d_m)m - \rho_1 m$		
	m: Monocyte concentration	d_m:	Monocyte diffusion
	σ_w: Wall shear stress	ρ_1:	Monocytes differentiation
	L_{ox}: Ox-LDL		
Mckay *et al.*[64]	$\frac{dm}{dt} = \rho_m C + (\mu - \rho_m) mP$		
	m: Monocytes density	μ:	Monocyte proliferation/differentiation
	ρ_m: Monocyte production/influx	P:	Proliferation factor density
	C: Chemo-attractant density		
El Khatib *et al.*[52,53] Ougrinovskaia *et al.*[71]	$\begin{cases} \frac{\partial M}{\partial t} = d_1 \frac{\partial^2 M}{\partial x^2} + f_1(A) - \lambda_1 M \\ \frac{\partial A}{\partial t} = d_2 \frac{\partial^2 A}{\partial x^2} + f_2(A) M - \lambda_2 A \end{cases}$		
	M: Immune cells density	$f_2(A)M$:	Cytokines production rate
	A: Cytokines density	$\lambda_1 M$:	Immune cells degradation
	$f_1(A)$: Immune cells recruitment	$\lambda_2 A$:	Cytokines degradation
Filipovic *et al.*[32]	$\partial_t O = d_1 \Delta O - k_1 O \cdot M$		
	O: Ox-LDL	k_1:	Solute lag coefficient
	d_1: Diffusion coefficient	M:	Macrophages concentration in the intima
Chalmers *et al.*[13]	$\frac{\partial p}{\partial t} = D_p \frac{\partial^2 p}{\partial x^2} + \mu_p \frac{lm}{1+l} - d_p p$		
	p: Chemoattractant concentration	l:	modLDL density
	D_p: Chemoattractant diffusion	m:	Macrophages density
	μ_p: Macrophages conversion rate		

Monocyte to Macrophage Differentiation

Macrophage formation after taking up oxLDL is described by a reaction term.[78] The evolution of oxLDL and the transformation of monocytes to macrophages were incorporated in the work of Calvez and Ebde[12] and Silva *et al.*[89] It was assumed that all monocytes would differentiate into macrophages once

TABLE 6. Summary of the governing equations used in monocyte to macrophage differentiation.

Reference	Governing equations		
Reddy and Seshaiyer[78]	$\begin{cases} \frac{\partial M}{\partial t} + \nabla \cdot (\mu M \nabla L) = D_M \nabla^2 M - k_M LM + f(L) \\ \frac{\partial N}{\partial t} = k_M LM - k_N N \end{cases}$		
	M: Macrophages concentration	k_M:	Macrophages reaction rate
	μ: chemotactic sensitivity coefficient	$f(L)$:	Macrophage influx
	L: LDL/ox-LDL concentration	N:	Necrotic lipids concentration
	D_M: Macrophages diffusion coefficient	k_N:	Plaque destruction rate
Calvez and Ebde[12]	$\partial_t M + \mathrm{div}(\upsilon M) = d_2 \Delta M - k_1 Ox \cdot M$		
	M: Macrophages density	k_1:	Macrophage creation term
	υ: Monocyte displacement speed	Ox:	Ox-LDL density
	d_2: Signal diffusion constant		
Cilla *et al.*[19]	$\frac{\partial C_{m,w}}{\partial t} + \nabla \cdot \left(-D_{m,w} \nabla C_{m,w}\right) = d_m C_{m,w} - \frac{M_{r1}}{M_{r2}} LDL_{oxr} C_{m,w} C_{LDL_{ox},W}$		
	$C_{m,w}$: Monocytes concentration	M_{r2}:	Foam cell formation
	$D_{m,w}$: Monocytes diffusion	LDL_{oxr}:	Ox-LDL uptake
	d_m: Monocytes differentiation	$C_{LDL_{ox},W}$:	Ox-LDL
	M_{r1}: Ox-LDL to foam cell		
Hao and Friedman[42]	$\frac{\partial M}{\partial t} + \nabla \cdot (uM) - D_M \Delta M = -\nabla \cdot (M \chi_C \nabla P) + \lambda_{MI_\gamma} M \frac{I_\gamma}{I_\gamma + KI_\gamma} - d_M M$		
	M: Macrophage density	P:	MCP-1 density
	u: Cells common velocity	λ_{MI_γ}:	Activation rate of macrophages
	D_M: Macrophage diffusion coefficient	I_γ:	IFN-c concentration
	χ_C: Chemotactic sensitivity parameter	d_M:	Macrophage death rate
Tomaso *et al.*[99]	$M_0 = k_c \cdot r_w \cdot c_w$		
	M_0: Macrophages density	r_w:	LDL degradation rate
	k_c: Production of proinflammatory cytokines		
Chalmers *et al.*[13]	$\frac{\partial m}{\partial t} = D_m \frac{\partial^2 m}{\partial x^2} - \chi_m \frac{\partial}{\partial x}\left(m \frac{\partial I}{\partial x}\right) - \mu_m \frac{Im}{1+I} + \theta v_N \frac{hN}{\kappa + h} - d_m m$		
	m: Macrophages density	θ:	Foam cell proportion transformed to macrophages
	D_m: Macrophages random movement	v_N:	Foam cell flux
	χ_m: Chemotactic term	h:	HDL density
	I: modLDL density	N:	Foam cell density
	μ_m: Macrophages conversion rate	κ:	HDL saturation constant

inside the arterial wall and the recruitment of new monocytes depends on a general pro-inflammatory signal S. Based on the hypothesis that macrophages are relatively free to travel inside the tissue, their convection is much smaller than their diffusion. Cilla *et al.*[19] used a diffusion equation to describe the evolution of macrophages including foam cells apoptosis. The macrophages diffusion coefficient in the arterial wall was equal to the monocyte diffusion coefficient. A similar approach was followed in other studies.[31,45,53] A slightly more complicated expression was proposed by Hao and Friedman[42] including both chemotaxis due to MCP-1 and activation of macrophages due to IFM-γ. Tomaso *et al.*[99] used a constant source to model monocyte penetration through the endothelium based on previous work Tedgui and Lever,[98] assuming all monocytes differentiate into macrophages. Finally, Chalmers *et al.*[13] assumed that only a proportion of macrophages convert to foam cells and a proportion (θ) of foam cells revert to macrophages due to the presence of HDL. Table 6 recaps the governing equations used in monocyte to macrophage differentiation.

Foam Cell Formation and Accumulation

Calvez and Ebde[12] mathematically described foam cell production through a simple mass action law disregarding foam cell diffusion due to their relatively large size. In their work SMCs and fibers contribution to the inflammation is neglected, thus no reaction term was included in the biomass transport equation. Cilla *et al.*[19] modeled macrophages apoptosis using a reaction term along with no-flux boundary conditions at the artery walls, and a similar approach was presented by Tomaso *et al.*[99] Hao and Friedman[42] also modeled the production and death of foam cells using a PDE. In the work of Chalmers *et al.*[13] the inflammation procedure was modeled including cytokine production after macrophages take up ox-LDL. In addition to the foam cell formation, the non-inflammatory process was also included due to the presence of HDL and the subsequent removal of the lipid core.

A transport equation was used by Yang *et al.*[106] for macrophages motion in the vessel wall with a reaction term representing the foam cells formation. In addi-

TABLE 7. Summary of the governing equations used in foam cell formation and accumulations.

Reference	Governing equations			
Calvez and Ebde[12]	$\partial_t F + \mathrm{div}(\upsilon F) = k_1 Ox \cdot M$			
	F:	Foam cells density	Ox:	Ox-LDL density
	υ:	Monocyte displacement speed	M:	Macrophages density
	k_1:	Macrophage creation term		
Cilla *et al.*[19]	$\frac{\partial C_{F,w}}{\partial t} = \frac{M_{r1}}{M_{r2}} LDL_{oxr} C_{m,w} C_{LDL_{OX},W}$			
	$C_{F,w}$:	Foam cells concentration	LDL_{oxr}:	Ox-LDL uptake
	M_{r1}:	Ox-LDL to foam cell	$C_{m,w}$:	Monocytes concentration
	M_{r2}:	Foam cell formation	$C_{LDL_{OX},W}$:	Ox-LDL diffusion
Hao and Friedman[42]	$\frac{\partial F}{\partial t} + \nabla \cdot (uF) - D_F \Delta F = \lambda_{FM} \frac{L_{ox}}{K_{L_{ox}} + L_{ox}} M - d_F F$			
	F:	Foam cells density	L_{ox}:	ox-LDL density
	u:	Cells common velocity	$K_{L_{ox}}$:	ox-LDL saturation for production of MCP-1
	D_F:	Foam cells diffusion coefficient	M:	Macrophages density
	λ_{FM}:	Foam cells activation rate	d_F:	Foam cell death rate
Chalmers *et al.*[13]	$\frac{\partial N}{\partial t} = D_N \frac{\partial^2 N}{\partial x^2} + \mu_m \frac{lm}{1+l} - \nu_N \frac{hN}{\kappa + h}$			
	N:	Foam cell density	m:	Macrophages density
	D_N:	Foam cells random movement	ν_N:	Foam cell flux
	μ_m:	Macrophages conversion rate	h:	HDL density
	l:	modLDL density	κ:	HDL saturation constant
Yang *et al.*[106]	$\frac{\partial c_s^*}{\partial t} + \mathrm{div}(c_s^* v_s) = f_s^r$			
	c_s^*:	Foam cells concentration	f_s^r:	Foam cells production rate
	u_s:	Vessel wall velocity		
Bulelzai and Dubbeldam[11]	$\frac{dF}{dt} = \frac{\rho_{in} L_{ox}}{1 + L_{ox}/L_{th}} M$			
	F:	Foam cells concentration	L_{ox}:	Ox-LDL concentration
	ρ_{in}:	1.15×10^{-6} s^{-1}	M:	Macrophage concentration

tion, a balance equation for the macrophage accumulation was used. A key feature of the model is that the mechanical properties of the plaque change as a result of foam cells concentration. Moreover, a linear dependence of the reaction function on the macrophages concentration and the growth function on the reaction rate was assumed.

Bulelzai and Dubbeldam[11] presented their model regarding the formation of foam cells following ox-LDL uptake by macrophages. The proposed model adopts similar approaches as in previous studies.[21,71] Ougrinovskaia *et al.*[71] proposed a model neglecting small timescale events for the lesion development without incorporating cap formation. In their work qualitative properties of the lesions instead of specific concentration of the different factors were adopted. Michaelis–Menten kinetics were used for ox-LDL uptake by macrophages. Another common point is the use of a sigmoidal function for the saturating uptake rate. Cohen *et al.*[21] model studied the HDL effect in atherosclerosis, nevertheless, the rest of the equations were the same as in Ougrinovskaia *et al.*[71] A synopsis of the governing equations used in foam cell formation and accumulations is tabulated in Table 7.

T Cell Recruitment and the Role of Interferon-Gamma (IFN-γ)

In most studies, the role of T-cells is rarely investigated. A very detailed approach was presented by Hao and Friedman.[42] In their work, an equation for T-cells density was presented expressing T-cells activation by IL-12. The effect of IL-1 and IL-6, which are produced by macrophages and SMCs, was also taken into consideration. In addition, the IFN-γ production related to T-cells and the subsequent degradation, as well as the concentration of interleukin-12, were modeled. In their work values of all necessary parameters are tabulated. A similar approach was adopted by Friedman and Hao[34] in their model for reverse cholesterol transport impact. Table 8 summarises the governing equations used in T cell and IFN-γ recruitment.

Proliferation of SMCs

Another scarcely studied factor is the role of the SMCs in atherosclerosis.

A detailed study of the role of SMCs was presented by Hao and Friedman[42] considering the PDGF secretion by SMCs amongst other cells, ECM remodelling due to the matrix metalloproteinase (MMP) and tissue inhibitor of metalloproteinase (TIMP) produced by SMCs amongst other cells. A set of complementary reaction–diffusion equations for the formation of PDGF, MMP, and TIMP was presented. Values of the parameters used in the simulations were derived from the literature.

In contrast, Cilla *et al.*[19] neglected diffusion and convection terms of the differential equation of SMCs behavior due to their large size and because

TABLE 8. Summary of the governing equations used in T cell and IFN-γ recruitment.

Reference	Governing equations
Hao and Friedman[42]	$\begin{cases} \frac{\partial T}{\partial t} + \nabla \cdot (uT) - D_T \Delta T = \lambda_{TI_{12}} \frac{M}{K_M + M} I_{12} - d_T T \\ \frac{\partial I_\gamma}{\partial t} - D_{I_\gamma} \Delta I_\gamma = \lambda_{I_\gamma T} T - d_{I_\gamma} I_\gamma \\ \frac{\partial I_{12}}{\partial t} - D_{I_{12}} I_{12} = \lambda_{I_{12}M} \frac{M}{K_M + M} \left(1 + \frac{I_\gamma}{K_{I_{12}} H + I_\gamma}\right) + \lambda_{I_{12}F} \frac{F}{K_F + F} - d_{I_{12}} I_{12} \end{cases}$

T:	Density of T cells	I_γ:	Concentration of IFN-γ
u:	Cells common velocity	D_{I_γ}:	Degradation rate of IFN-γ
D_T:	Diffusion coefficient of T cell	$\lambda_{I_\gamma T}$:	Production rate of IFN-γ by T cells
$\lambda_{TI_{12}}$:	Activation rate of T cells by IL-12	$D_{I_{12}}$:	Degradation rate of IL-12
M:	Macrophages density	$\lambda_{I_\gamma M}$:	Production rate of IFN-γ by Macrophages
K_M:	Macrophages saturation	$K_{I_{12}}$:	IFN-γ saturation for production of IL-12
I_{12}:	Concentration of IL-12	H	Concentration of HDL
d_T:	Death rate of T cell	$\lambda_{I_{12}F}$:	Production rate of IL-12 by foam cells

TABLE 9. Summary of the governing equations used in SMCs proliferation.

Reference	Governing equations
Hao and Friedman[42]	$\begin{cases} \frac{\partial S}{\partial t} + \nabla \cdot (uS) - D_S \Delta S = -\nabla \cdot (S \chi_C \nabla P) - \nabla \cdot (S \chi_C \nabla G) - \nabla \cdot (S \chi_H \nabla \rho) \\ \frac{\partial G}{\partial t} - D_G \Delta G = \lambda_{GM} M + \lambda_{GF} F + \lambda_{GF} S - d_G G \\ \frac{\partial Q}{\partial t} - D_Q \Delta Q = \lambda_{QS} S + d_{QQr} Q_r Q - d_Q Q \end{cases}$

S:	SMCs density	λ_{GF}:	Production rate of PDGF by foam cells
u:	Cells common velocity	F:	Foam cells density
D_S:	SMCs diffusion coefficient	d_G:	PDGF degradation rate
χ_C:	Chemotactic sensitivity parameter	Q:	MMPs density
P:	MCP-1 density	D_Q:	MMP diffusion coefficient
G:	PDGF density	λ_{QS}:	Production rate of MMP by SMCs
ρ:	ECM density	d_{QQr} :	Binding rate of MMP to TIMP
D_G:	PDGF diffusion coefficient	Q_r:	TIMP density
λ_{GM}:	Production rate of PDGF by macrophages	d_Q:	TIMP degradation rate
M:	Macrophages density		

Cilla *et al.*[19]

$$\begin{cases} \frac{\partial C_{S_c,w}}{\partial t} = -C_{S_c,w}(1 + \exp\frac{-S_r C_{c,w}}{C^{th}_{c,w}}) \\ \frac{\partial C_{S_S,w}}{\partial t} = -C_{S_c,w}\left(1 + \exp\frac{-S_r C_{c,w}}{C^{th}_{c,w}}\right) + C_{Ss,w} \frac{C_{c,w}}{C^{th}_{c,w}} m_{S_s} \end{cases}$$

$C_{S_c,w}$:	Contractile SMC concentration	$C^{th}_{c,w}$:	Maximum concentration of cytokines
S_r:	Contractile SMCs differentiation	$C_{Ss,w}$:	Synthetic SMC concentration
$C_{c,w}$:	Cytokines concentration	m_{S_s}:	SMCs migration rate
$C_{S_S,w}$:	Synthetic SMC concentration		

TABLE 10. Summary of the governing equations used in the collagen formation.

Reference	Governing equations
Mckay *et al.*[64]	$\frac{dG}{dt} = \rho_G S - d_G G$

Parameters

G:	Collagen density	d_G:	Collagen degradation
ρ_G:	Collagen production from SMC's		

Cilla *et al.*[19]

$$\frac{\partial C_{G,w}}{\partial t} = G_r C_{S_S,w} - d_G C_{G,w}$$

$C_{G,w}$:	Collagen concentration	$C_{S_S,w}$:	Synthetic SMC concentration
G_r:	Collagen secretion rate	d_G:	Collagen degradation rate

they do not spread due to diffusion. Model parameters, such as concentration and passing rate into the intima were depicted in the literature along with appropriate boundary conditions.[38,107] A similar approach was adopted by Mckay *et al.*[64] and Ibragimov *et al.*[45] Summary of the governing equations used in SMCs proliferation is shown in Table 9.

TABLE 11. Summary of the governing equations used in the 2D atherosclerotic plaque growth models.

Reference	Governing equations		
Zohdi *et al.*[112]	$\dot{\alpha} = K\eta$		
	Parameters		
	$\dot{\alpha}$: Intimal thickness	η:	Particle adhesion distribution function
	K: Intimal growth rate constant		
Bulelzai and Dubbeldam[11]	$V(t+\Delta t) = V(t) + \left(v_M \frac{dM}{dt} + v_{Lox} \frac{dLox}{dt} + v_m \frac{dm}{dt} + v_F \frac{dF}{dt}\right) V(t)\Delta t$		
	v_m= 10^{-17} m^3		
	$V(t)$: Plaque volume	M:	Macrophage concentration
	v_M: 10^{-14} m^3	Lox:	Ox-LDL
	v_{Lox}: 10^{-21} m^3	m:	Monocyte concentration
	v_F: 10^{-13} m^3	F:	Foam cells concentration
Fok[33]	$\dot{R} = -\frac{\alpha\sigma[R;\theta_0(0)]C_1(\lambda_1,\lambda_2)}{R\Delta_0(R)} + \frac{1}{2}\left(\frac{1-R^2}{R}\right) - \frac{\beta\sigma[R;\theta_0(0)]}{R\Delta_0(R)\lambda_1}\{C_2(\lambda_1,\lambda 2)[RK_1(\lambda_1 R) - K_1(\lambda_1)] - C_3(\lambda_1,\lambda_2)[RI_1(\lambda_1 R) - I_1(\lambda_1)]\}$		
	α: Chemotactic parameter	λ_1, λ_2:	Steady-state diffusion–degradation parameters
	β: Proliferation parameter	$I_1(\cdot), K_1(\cdot)$:	Modified Bessel functions
	$\theta_0(0)$: Initial angle of injury	C_1, C_2, C_3:	constants
Silva *et al.*[89]	$\frac{dh}{dt} = \frac{k_1}{Ah} Q_{ox} \cdot Q_M$		
	h New intima's height	Q_{ox}	0.25 g·cm^{-1}
	k_1 1 cm·(g^{-1}s^{-1})	Q_M	0.1
	A 1 g·cm^{-3}		
Gabriel *et al.*[35]	$\boldsymbol{x}^{j+1} = \boldsymbol{x}^j + f_g \max\left\{\frac{Kc_w - K_0 c_c}{K_0 c_c}, 0\right\}\boldsymbol{n}$		
	$\boldsymbol{x}$: Material point displacement	c_w:	LDL concentration
	f_g: Multiplicative factor	K_0:	Normal flow permeability
	K: Endothelial wall's LDL permeability coefficient	c_c:	1.2
		$\boldsymbol{n}$:	local surface normal
Hao and Friedman[42]	Plaque weight = $(M + F + S + T)\mathrm{d}\Omega$		
	M: Macrophage density	S:	SMCs density
	F: Foam cells density	T:	T cells density
Yang *et al.*[106]	$\begin{cases} f_s^r = \beta c_s \\ f_s^g = \gamma f_s^r \end{cases}$ in Ω_s^t		
	f_s^r: Foam cells accumulation	f_s^g:	Plaque growth function
	β: coefficient	γ:	constant
	c_s: Foam cells concentration		

Collagen Formation

The formation of collagen, the extracellular matrix created by the SMCs, was described in the work of Mckay *et al.*[64] using production and degradation rates. The process of collagen formation was also included in Cilla *et al.*[19] model simplified the biochemical process by neglecting the diffusion and the convection terms, thus leaving only the secretion and the degradation rates using values presented in the literature. Details of the governing equations used in the collagen formation are depicted in Table 10.

Atherosclerotic Plaque Growth and Rupture

Atherosclerotic plaque fate has been extensively studied so far. Atherosclerosis growth could be categorised based on whether they use ODEs or PDEs with the vast majority of the models incorporating PDEs whereas only a small fraction entails ODEs.[11,20,21,45,71,108,111] Following, a comprehensive analysis of plaque growth models and their simplifications, modelling is presented categorised as 2D and 3D.

Two-dimensional models, tabulated in Table 11, are the majority of the published work so far addressing progress and growth of the atherosclerotic plaque. What is common among all existing studies is the great number of simplifications applied to these models. Nevertheless, some striking features are noticed concerning the methodology followed by the authors. As such, one of the first studies correlated arterial plaque growth with a growth rate constant derived from empirical data, material properties, and the monocytes accumulation in the arterial wall.[112] The study also proposed that the fibrous cap rupture could be described in terms of stored energy occurring at a critical time that depends on the value of the hydrostatic pressure; when the pressure exceeds a threshold, rupture occurs. Another approach was presented by Li

et al.[58] suggesting that Arbitrary Lagrangian–Eulerian (ALE) and Ogden strain energy methodologies could describe the fluid flow and plaque structure interplay. Some of the simplifications of this work are the use of concentric plaque geometry, the lack of morphological accurate factors such as the lipid core due to macrophages, and finally the vessel geometry. Fazli *et al.*[29] indicated that the growth rate of the plaque is not linear with time and the rate is high in the beginning, then it becomes smaller and finally it increases again but not as much as the growth rate in the beginning. A few years later, a modified version of the model by Zohdi *et al.*[112] including macrophages, ox-LDL, monocytes and foam cells was published by Bulelzai and Dubbeldam.[11] disregarding the role of SMCs and collagen in the plaque formation and growth. A completely different approach was presented by Fok[33]; a single ordinary differential equation free of boundary conditions to describe the evolution of arterial stenosis driven by the SMCs flux from the media, their proliferation, and subsequent death. Other recent studies proposed a 1D model of lesion growth assuming ECM, smooth cells and other biological factors do not participate in the inflammatory process and a temporal scale-independent model without mass conservation in the lesion and only LDL mass transport considered.[35,89] One of the more comprehensive models was proposed by Hao and Friedman[42] where the plaque weight estimation includes the macrophages, the T-cells, the foam cells, the SMCs, and the ECM density. Finally, one of the latest works employed the ALE method to solve the equations in both the fluid and the solid domain one of the key features of the results was the observation of a two-humps plaque shape instead of a bell-shaped one.[106] Despite the capability to simulate the plaque growth, several biochemical factors were disregarded, and the vessel wall density was assumed to be a constant value, independent of time.

On the other hand, 3D models are scarce. The governing equations used in the 3D atherosclerotic plaque growth models are tabulated in Table 12. One of the first attempts proposed a 3D model with a plaque growth function calculating the increase of the wall thickness.[61] The linear function implemented two constants representing the relation between coronary artery diameter change and wall shear stress in a 3-year period, and the time-averaged wall shear stress. In general, this model has limited applicability since it could only serve for simulating the plaque initiation. Filipovic *et al.*[32] correlated intimal thickening to the shear stress via a system of PDEs simulating the inflammatory process. In order to follow the change of the vessel wall geometry during plaque growth, a 3D mesh moving algorithm was applied. They also simplified the inflammatory process disregarding smooth muscle cell proliferation and foam cells formation including only ox-LDL, macrophages, and cytokines. Another approach correlates growth of the plaque to the accumulation of foam cells, SMCs, and collagen.[19] The velocity of the growth was related to the variation of SMCs, the volume of the spherical foam cells and the ellipsoidal SMCs. Finally, one of the latest multiscale models utilises the occupied volume due to the foam cells stratification, the volume of the accumulated foam cells, and the portion of endothelium in the fatty streak formation.[99,100] A threshold of 1% was set as the maximum arterial wall deformation without significant impact on the blood flow dynamics.

The validation of the aforementioned models is also important and the relevant information in the corresponding studies is shown in Table 13.

TABLE 12. Summary of the governing equations used in the 3D atherosclerotic plaque growth models.

Reference	Governing equations			
Liu and Tang[61]	$\mathrm{WTI} = K_1 - K_2\tau$			
	WTI:	Wall thickness increase	K_2:	Constant
	K_1:	constant	τ:	Time-averaged WSS
Filipovic *et al.*[32]	$\partial_t M + \mathrm{div}(v_w M) = d_2\Delta M - k_1 O \cdot M + S/(1+S)$			
	M:	Macrophages concentration	k_1:	Solute lag coefficient
	u_w:	Inflammatory velocity	O:	Ox-LDL
	d_2:	Diffusion coefficient	S:	Cytokines concentration
Cilla *et al.*[19]	$\nabla \cdot u = \frac{\partial C_{F,w}}{\partial t}\mathrm{Vol}_{\mathrm{foamcell}} + \frac{\partial \Delta C_{S,w}}{\partial t}\mathrm{Vol}_{\mathrm{SMC}} + \frac{\partial C_{G,w}}{\partial t}\frac{1}{\rho_G}$			
	u:	Material points velocity	$\mathrm{Vol}_{\mathrm{SMC}}$:	SMC volume
	$C_{F,w}$:	Foam cells concentration	$C_{G,w}$:	Collagen concentration
	$\mathrm{Vol}_{\mathrm{foamcell}}$:	Foam cell volume	ρ_G:	Collagen density
	$\Delta C_{S,w}$:	SMCs variation		
Tomaso *et al.*[99,100]	$\Delta h = \frac{V_F - V}{A_{\mathrm{tot}}}$			
	Δh:	Intima-media thickness growth	V:	Accumulated foam volume
	VF:	Wound model foam cells stratification	A_{tot}:	Portion of endothelium

TABLE 13. Summary of validation information of atherosclerosis initiation and progression models.

Reference	Validation
Bulelzai and Dubbeldam[11]	Results were in contrast with results presented by Zohdi *et al.*[112]
Calvez and Ebde[12]	Results were in contrast with results presented by Zohdi *et al.*[112] This divergence was attributed to the differences in the uptake mechanisms of LDL particles.
Silva *et al.*[89]	No validation
Gessaghi *et al.*[36]	The model reproduces qualitatively few aspects of early stage lesions such as wall thickness increase and identify prone areas when compared with experimental data of Guyton and Klemp[39] and Homma *et al.*[44]
Reddy and Seshaiyer[78]	No validation
Cilla *et al.*[19]	LDL concentration at the low WSS areas of the arterial wall was reported to be in good agreement with published experimental results by Meyer *et al.* and qualitatively predicts evolution of stenosis when compared with results by Achenbach[1]
Hao and Friedman[42]	No validation
Friedman and Hao[34]	Simulation results were in qualitative agreement with Rayner *et al.*[77] for plaque regression using anti-miR33 treatment, with experimental results of Schiopu *et al.*[82] on plaque weight, with Panousis *et al.*[72] regarding ABCA1 increase when using TGF-β treatment and with Lovren *et al.*[62] for plaque growth decrease when miR-145 was used to target SMCs.
Mckay *et al.*[64]	No validation
Filipovic *et al.*[31]	Besides the lesion shape LDL distribution in low WSS area was found in good agreement with plaque composition experimental results by Cheng *et al.*[16]
El Khatib *et al.*[52,53]	No validation
Ougrinovskaia *et al.*[71]	Qualitative comparison of simulation results with studies of Ibragimov *et al.*,[45] Libby and Ridker,[59] Libby *et al.*[60]
Filipovic *et al.*[32]	Qualitative comparison with plaque geometry obtained from image reconstruction.
Chalmers *et al.*[13]	Model predictions agree qualitatively with experimental studies in mice and rabbits presented by Feig *et al.*[30] and the work of Rohatgi *et al.*[80]
Yang *et al.*[106]	No validation
Zohdi *et al.*[112]	Authors state good qualitative agreement of the simulations with observations
Fok[33]	Comparison with experimental data from Stadius *et al.*[92]
Liu and Tang[61]	Plaque growth estimated rate is consistent with results presented by Stone *et al.*[95]
Tomaso *et al.*[99,100]	Model predictions were in good agreement with in vivo observations from multislice computed tomography (MSCT)

PERSPECTIVES AND CHALLENGES

All the aforementioned mathematical models incorporate simplifications regarding the biochemical processes involved in the lesion formation and the atheromatous plaque progress. Nevertheless, the computational procedure is based on several parameters regarding cell dynamics, such as diffusion and concentration. Despite the fact that additional experiments are needed so as to fine tune several of these parameters, it should be also noted that these parameters cover only a fraction of the biochemical processes involved in the development of the lesion. The interplay of other factors such as triglycerides, HDL, B cells, sterol regulatory elements, signaling proteins has not yet been sufficiently described by mathematical equations or computational models. Even though a significant amount of work is published so far regarding the build-up of the plaque, this could only be considered as the tip of the iceberg. Consequences of the progression of the atheromatous plaque such as plaque rupture due to its vulnerability to the subjected stresses and subsequent thrombus formation are still unexplored since only few studies are published presenting concise results. In view of this, the purpose of the scientific community to suggest a reliable tool to predict areas of the vasculature prone to developing atheromatous plaque and, at the same time, predict the risk of huge plaque rupture posing life-threatening consequences to the patient, remains largely unfulfilled.

Despite the huge efforts that have been made so far, a lot of uncertainties exist and should be convincingly clarified before pursuing a more complete multiscale computational platform. Next, we attempt to briefly point out some of these uncertainties in the present state of the art.

First, the nature of the blood and the subsequent modelling method is very important. Part of the published studies model blood as a Newtonian fluid, whereas others prefer non-Newtonian approach. Recent studies comparing available blood rheological models demonstrated some of the misconceptions when performing cardiovascular simulations. Skiadopoulos *et al.*[91] concluded that WSS distribution pattern is unconstrained by the rheological model

contrarily to its magnitude and oscillations, which is in accordance with Ai and Vafai.[2] In their work, it was found that Newtonian model performs satisfactorily in high shear and flow rates, but the formation of atheromatous lesions is overestimated in areas where WSS exhibits an oscillating nature. Another aspect related to the blood flow nature is the development of the recirculation zone and the impact on WSS distribution in cases of large stenosis. It was shown by Nematollahi *et al.*[67] that the recirculation zone in arteries with severe stenosis, and the decrease of WSS in the reattachment points, which favors disease progress, is inadequately modeled with a Newtonian approximation. Similar findings were presented by Millon *et al.*,[65] stressing the existence of atherosclerotic lesions in the segment after the stenosis and not before, which was correlated with the low WSS distribution in the post-stenosis area. It has been also stressed that the recirculation zones generated by the plaque development and the ongoing change of the blood flow profile are related to phenomena that are indicative of possible plaque rupture. Such phenomena are delamination and erosion, yet there is no solid evidence for their dependency on WSS distribution.[7] Nevertheless, Non-Newtonian constitutive equations for blood tend to Newtonian behavior at high shear rates and therefore their use makes sense for shear rates typically lower than 50 s^{-1}, at which the residence time of red blood cells—a key aspect of Non-Newtonian behavior—should be taken into account.[5]

Secondly, the introduction of more realistic geometries would greatly favor blood flow assessment, the interconnected onset of the inflammatory process, and the disease progress. Up-to-date techniques enable the reconstruction of patient-specific geometries facilitating the observation of the cardiovascular disease in several conditions: disease-free and through several stages of the inflammatory process and subsequent plaque growth. The continuous progress in computed tomography coronary angiography is sought to elucidate the onset and progress of the disease with respect to interpatient and intrapatient variability. Differentiations of carotid, femoral, and coronary arteries amongst different patients will enhance prognosis of the prone regions due to different shear stress distribution, as well as the in-time evaluation of the plaque rupture risk. In addition, anatomical variations of the same type of artery in a group of patients would lead to more sophisticated model predictions since each vasculature region would respond differently in the blood flow dynamics.[14,55] This approach necessitates more accurate and patient-oriented boundary conditions of the blood flow and the mass transport since each patient profile varies because of the age, the lifestyle, or other underlying diseases.[24,81]

Thirdly, biological tissue's transport properties pose an additional challenge. To date, the multi-layer approach is the most common methodology to describe the arterial wall. The set of equations and the corresponding boundary conditions provide a realistic description of the biological tissue anatomy. Nonetheless, development of more sophisticated predictive tools is dependent to more accurate parameters involved in the biological transport phenomena, such as the permeability, the porosity, and the diffusivity. Likewise, other important factors are the upscale of animal experimental results to humans, the lack of human-tissue properties and the lack of information regarding the transition phase between normal and stenosed arteries.[50] Further advances in multiscale modelling tools depend on data regarding cell -population dynamics, lipid-core formation, and fibrous cap as well as plaque rupture.[106] In this context, a suggested option is to modify the four-layer model to account for the glycocalyx effect or the artery wall layers thickness variability thus yielding a more sophisticated model for the plaque morphology in the circumferential and vertical direction.[49,106]

Finally, a significant goal is the establishment of an equilibrium state via modifying either the macrophage or the HDL influx or reduce LDL levels by using statins. Early findings suggest that plaque regression could be facilitated,[8,9] and an equilibrium could be achieved if the macrophage influx is modified at its early stage. Identification of such a time window is crucial since macrophage influx reduction in a later stage of the atheromatous progression would only result in a slower growth rate.[21,22,57,66] Another aspect of the atherosclerosis disease study with increasing interest is the plaque growth regression due to HDL particles mimicking high lipid proteins.[4,86,97,110] Purpose of these studies was to examine the ability to achieve plaque equilibrium at its early stage when its size is relatively small. On the other hand, results have shown that efforts to engineer the fate of a larger plaque are less effective. Modelling studies incorporating HDL effect are scarce to date.[21,34] Recently, Friedman and Hao[34] predicted plaque weight and macrophage density decline because of increase in HDL efficiency, however, no equilibrium was reached. Authors noted that the plaque regression observed in clinical studies with animals is not observed in human clinical studies with a late-stage plaque of complicated structure. Future work should address the efficacy of HDL increase towards achieving plaque equilibrium in patients with early-stage plaque, adding more clinical evidence regarding patients with late-stage atheromatous plaque and already suffering from subsequent symptoms.

CONCLUSIONS

Despite the great effort been made so far, it is not yet possible to comprehensively predict or re-engineer the fate of atherosclerosis. Close cooperation by experts from different sectors such as medicine, engineering, physics, and chemistry in this multidisciplinary problem would seek more experimental research generating customised data for necessary parameters involved in particles transport inside the arterial wall. Consequently, modeling accuracy could be upgraded regarding arterial properties, blood flow dynamics, biochemical processes, and boundary conditions. This would be a crucial step towards *in silico* biomedical trials that are expected to have a deep impact to the patient quality of life, the medical procedures and the economics of cardiovascular diseases.

REFERENCES

[1]Achenbach, S. Quantification of coronary artery stenoses by computed tomography. *JACC Cardiovasc. Imaging* 1:472–474, 2008.

[2]Ai, L., and K. Vafai. An investigation of stokes' second problem for non-Newtonian fluids. *Numer. Heat Transf. Part A Appl.* 47:955–980, 2005.

[3]Ai, L., and K. Vafai. A coupling model for macromolecule transport in a stenosed arterial wall. *Int. J. Heat Mass Transf.* 49:1568–1591, 2006.

[4]Andrews, J., A. Janssan, T. Nguyen, A. D. Pisaniello, D. J. Scherer, J. J. P. Kastelein, B. Merkely, S. E. Nissen, K. Ray, G. G. Schwartz, S. G. Worthley, C. Keyserling, J.-L. Dasseux, J. Butters, J. Girardi, R. Miller, and S. J. Nicholls. Effect of serial infusions of reconstituted high-density lipoprotein (CER-001) on coronary atherosclerosis: rationale and design of the CARAT study. *Cardiovasc. Diagn. Ther.* 7:45–51, 2017.

[5]Arzani, A. Accounting for residence-time in blood rheology models: do we really need non-Newtonian blood flow modelling in large arteries? *J. R. Soc. Interface* 15:146, 2018.

[6]Arzani, A., A. M. Gambaruto, G. Chen, and S. C. Shadden. Wall shear stress exposure time: a Lagrangian measure of near-wall stagnation and concentration in cardiovascular flows. *Biomech. Model. Mechanobiol.* 16:787–803, 2017.

[7]Assemat, P., K. K. Siu, J. A. Armitage, S. N. Hokke, A. Dart, J. Chin-Dusting, and K. Hourigan. Haemodynamical stress in mouse aortic arch with atherosclerotic plaques: preliminary study of plaque progression. *Comput. Struct. Biotechnol. J.* 10:98–106, 2014.

[8]Badimon, J. J., L. Badimon, and V. Fuster. Regression of atherosclerotic lesions by high density lipoprotein plasma fraction in the cholesterol-fed rabbit. *J. Clin. Invest.* 85:1234–1241, 1990.

[9]Belalcazar, L. M., A. Merched, B. Carr, K. Oka, K.-H. Chen, L. Pastore, A. Beaudet, and L. Chan. Long-term stable expression of human apolipoprotein A-I mediated by helper-dependent adenovirus gene transfer inhibits atherosclerosis progression and remodels atherosclerotic plaques in a mouse model of familial hypercholesterolemia. *Circulation* 107:2726–2732, 2003.

[10]Bhalla, G., and W. M. Deen. Effects of charge on osmotic reflection coefficients of macromolecules in fibrous membranes. *Biophys. J.* 97:1595–1605, 2009.

[11]Bulelzai, M. A. K., and J. L. A. Dubbeldam. Long time evolution of atherosclerotic plaques. *J. Theor. Biol.* 297:1–10, 2012.

[12]Calvez, V., and A. Ebde. Mathematical modelling of the atherosclerotic plaque formation. *ESAIM Proc. CEMRACS 2008 - Model. Numer. Simul. Complex Fluids* 1–16, 2010. https://doi.org/10.1051/proc/2009036.

[13]Chalmers, A. D., C. A. Bursill, and M. R. Myerscough. Nonlinear dynamics of early atherosclerotic plaque formation may determine the efficacy of high density lipoproteins (HDL) in plaque regression. *PLoS ONE* 12:1–23, 2017.

[14]Chatzizisis, Y. S., A. U. Coskun, M. Jonas, E. R. Edelman, C. L. Feldman, and P. H. Stone. Role of endothelial shear stress in the natural history of coronary atherosclerosis and vascular remodeling.molecular, cellular, and vascular behavior. *J. Am. Coll. Cardiol.* 49:2379–2393, 2007.

[15]Chen, D., J. M. Roda, C. B. Marsh, T. D. Eubank, and A. Friedman. Hypoxia inducible factors-mediated inhibition of cancer by GM-CSF: a mathematical model. *Bull. Math. Biol.* 74:2752–2777, 2012.

[16]Cheng, C., D. Tempel, R. Van Haperen, A. Van Der Baan, F. Grosveld, M. J. A. P. Daemen, R. Krams, and R. De Crom. Atherosclerotic lesion size and vulnerability are determined by patterns of fluid shear stress. *Circulation* 113:2744–2753, 2006.

[17]Cheng, X., and P. M. Pinsky. The balance of fluid and osmotic pressures across active biological membranes with application to the corneal endothelium. *PLoS ONE* 10:1–18, 2015.

[18]Chien, S. Molecular and mechanical bases of focal lipid accumulation in arterial wall. *Prog. Biophys. Mol. Biol.* 83:131–151, 2003.

[19]Cilla, M., E. Pena, and M. A. Martinez. Mathematical modelling of atheroma plaque formation and development in coronary arteries. *J. R. Soc. Interface* 11:20130866, 2013.

[20]Cobbold, C. A., J. A. Sherratt, and S. R. J. Maxwell. Lipoprotein oxidation and its significance for atherosclerosis: a mathematical approach. *Bull. Math. Biol.* 64:65–95, 2002.

[21]Cohen, A., M. R. Myerscough, and R. S. Thompson. Athero-protective effects of high density lipoproteins (HDL): an ODE model of the early stages of atherosclerosis. *Bull. Math. Biol.* 76:1117–1142, 2014.

[22]Craeyveld, E., S. C. Gordts, E. Nefyodova, F. Jacobs, and B. De Geest. Regression and stabilization of advanced murine atherosclerotic lesions: a comparison of LDL lowering and HDL raising gene transfer strategies. *J. Mol. Med.* 89:555–567, 2011.

[23]Cunningham, K. S., and A. I. Gotlieb. The role of shear stress in the pathogenesis of atherosclerosis. *Lab. Investig.* 85:9–23, 2005.

[24]Dabagh, M., P. Jalali, and J. M. Tarbell. The transport of LDL across the deformable arterial wall: the effect of endothelial cell turnover and intimal deformation under hypertension. *Am J Physiol Heart Circ Physiol* 297:H983–H996, 2009.

[25]Díaz-Zuccarini, V., O. Agu, G. Di Tomaso, and C. Pichardo-Almarza. Towards personalised management of atherosclerosis via computational models in vascular clinics: technology based on patient-specific simulation approach. *Healthcare Technol. Lett*. 1:13–18, 2014.
[26]Farghadan, A., and A. Arzani. The combined effect of wall shear stress topology and magnitude on cardiovascular mass transport. *Int. J. Heat Mass Transf*. 131:252–260, 2019.
[27]Farid, A. S., and Y. Horii. Modulation of paraoxonases during infectious diseases and its potential impact on atherosclerosis. *Lipids Health Dis*. 11:1–15, 2012.
[28]Fatouraee, N., X. Deng, A. De Champlain, and R. Guidoin. Concentration polarization of low density lipoproteins (LDL) in the arterial system. *Ann. N. Y. Acad. Sci*. 858:137–146, 1998.
[29]Fazli, S., E. Shirani, and M. R. Sadeghi. Numerical simulation of LDL mass transfer in a common carotid artery under pulsatile flows. *J. Biomech*. 44:68–76, 2011.
[30]Feig, J. E., J. X. Rong, R. Shamir, M. Sanson, Y. Vengrenyuk, J. Liu, K. Rayner, K. Moore, M. Garabedian, and E. A. Fisher. HDL promotes rapid atherosclerosis regression in mice and alters inflammatory properties of plaque monocyte-derived cells. *Proc. Natl. Acad. Sci*. 108:7166–7171, 2011.
[31]Filipovic, N., D. Fotiadis, W. Pelosi, and O. Parodi. Experimental and computer model of plaque formation in the artery. *10th Int. Work. Biomed. Eng. BioEng 2011* 1–4, 2011. https://doi.org/10.1109/iwbe.2011.6079029.
[32]Filipovic, N., Z. Teng, M. Radovic, I. Saveljic, D. Fotiadis, and O. Parodi. Computer simulation of three-dimensional plaque formation and progression in the carotid artery. *Med. Biol. Eng. Comput*. 51:607–616, 2013.
[33]Fok, P. W. Mathematical model of intimal thickening in atherosclerosis: vessel stenosis as a free boundary problem. *J. Theor. Biol*. 314:23–33, 2012.
[34]Friedman, A., and W. Hao. A mathematical model of atherosclerosis with reverse cholesterol transport and associated risk factors. *Bull. Math. Biol*. 77:758–781, 2015.
[35]Gabriel, S. A., Y. Ding, Y. Feng, and J. A. Gear. Deposition-driven growth in atherosclerosis modelling. *19th Australas. Fluid Mech. Conf*. 1–5, 2014.
[36]Gessaghi, V. C., M. A. Raschi, D. Y. Tanoni, C. A. Perazzo, and A. E. Larreteguy. Growth model for cholesterol accumulation in the wall of a simplified 3D geometry of the carotid bifurcation. *Comput. Methods Appl. Mech. Eng*. 200:2117–2125, 2011.
[37]Gistera, A., and G. K. Hansson. The immunology of atherosclerosis. *Nat. Rev. Nephrol*. 13:368–380, 2017.
[38]Griffin, C. A., L. H. Apponi, K. K. Long, and G. K. Pavlath. Chemokine expression and control of muscle cell migration during myogenesis. *J. Cell Sci*. 123:3052–3060, 2010.
[39]Guyton, J. R., and K. F. Klemp. Transitional features in human atherosclerosis. Intimal thickening, cholesterol clefts, and cell loss in human aortic fatty streaks. *Am. J. Pathol*. 143:1444–1457, 1993.
[40]Hansson, G. K. Inflammation, atherosclerosis, and coronary artery disease. *N. Engl. J. Med*. 352:1685–1695, 2005.
[41]Hansson, G. K., A.-K. L. Robertson, and C. Söderberg-Nauclér. Inflammation and atherosclerosis. *Annu. Rev. Pathol. Mech. Dis*. 1:297–329, 2006.
[42]Hao, W., and A. Friedman. The LDL-HDL profile determines the risk of atherosclerosis: a mathematical model. *PLoS ONE* 9:1–15, 2014.
[43]Hodson, S., and R. Earlam. The incorporation of gel pressure into the irreversible thermodynamic equation of fluid flow in order to explain biological tissue swelling. *J. Theor. Biol*. 163:173–180, 1993.
[44]Homma, S., N. Hirose, H. Ishida, T. Ishii, G. Araki, and J. H. Halsey. Carotid plaque and intima-media thickness assessed by B-mode ultrasonography in subjects ranging from young adults to centenarians editorial comment. *Stroke* 32:830–835, 2001.
[45]Ibragimov, A. I., C. J. McNeal, L. R. Ritter, and J. R. Walton. A mathematical model of atherogenesis as an inflammatory response. *Math. Med. Biol*. 22:305–333, 2005.
[46]Karner, G., and K. Perktold. Effect of endothelial injury and increased blood pressure on albumin accumulation in the arterial wall: a numerical study. *J. Biomech*. 33:709–715, 2000.
[47]Kedem, O. A physical interpretation of the phenomenological coefficients of membrane permeability. *J. Gen. Physiol*. 45:143–179, 1961.
[48]Kedem, O., and A. Katchalsky. Thermodynamic analysis of the permeability of biological membranes to non-electrolytes. *Biochim. Biophys. Acta* 27:229–246, 1958.
[49]Kenjeres, S., and A. de Loor. Modelling and simulation of low-density lipoprotein transport through multi-layered wall of an anatomically realistic carotid artery bifurcation. *J. R. Soc. Interface* 11:20130941, 2013.
[50]Khakpour, M., and K. Vafai. Critical assessment of arterial transport models. *Int. J. Heat Mass Transf*. 51:807–822, 2008.
[51]Khaled, A.-R. A., and K. Vafai. The role of porous media in modeling flow and heat transfer in biological tissues. *Int. J. Heat Mass Transf*. 46:4989–5003, 2003.
[52]El Khatib, N., S. Génieys, B. Kazmierczak, and V. Volpert. Mathematical modelling of atherosclerosis as an inflammatory disease. *Philos. Trans. A. Math. Phys. Eng. Sci*. 367:4877–4886, 2009.
[53]El Khatib, N., S. Génieys, and V. Volpert. Atherosclerosis initiation modeled as an inflammatory process. *Math. Model. Nat. Phenom*. 2:126–141, 2007.
[54]Kolandavel, M. K., E. T. Fruend, S. Ringgaard, and P. G. Walker. The effects of time varying curvature on species transport in coronary arteries. *Ann. Biomed. Eng*. 34:1820–1832, 2006.
[55]Lee, J. M., G. Choi, D. Hwang, J. Park, H. J. Kim, J. H. Doh, C. W. Nam, S. H. Na, E. S. Shin, C. A. Taylor, and B. K. Koo. Impact of longitudinal lesion geometry on location of plaque rupture and clinical presentations. *JACC Cardiovasc. Imaging* 10:677–688, 2017.
[56]Li, L.-Y. Transport of multicomponent ionic solutions in membrane systems. *Philos. Mag. Lett*. 84:593–599, 2004.
[57]Li, R., H. Chao, K. W. S. Ko, S. Cormier, C. Dieker, E. A. Nour, S. Wang, L. Chan, and K. Oka. Gene therapy targeting LDL cholesterol but not HDL cholesterol induces regression of advanced atherosclerosis in a mouse model of familial hypercholesterolemia. *J. Genet. Syndr. Gene Ther*. 106:1–22, 2012.
[58]Li, Z. Y., S. P. S. Howarth, T. Tang, and J. H. Gillard. How critical is fibrous cap thickness to carotid plaque stability? A flow-plaque interaction model. *Stroke* 37:1195–1199, 2006.
[59]Libby, P., and P. M. Ridker. Inflammation and atherothrombosis. From population biology and bench research to clinical practice. *J. Am. Coll. Cardiol*. 48:A33, 2006.

[60]Libby, P., P. M. Ridker, and A. Maseri. Inflammation and atherosclerosis. *Circulation* 105:1135–1143, 2002.
[61]Liu, B., and D. Tang. Computer simulations of atherosclerotic plaque growth in coronary arteries. *Mol. Cell Biomech.* 7:193–202, 2010.
[62]Lovren, F., Y. Pan, A. Quan, K. K. Singh, P. C. Shukla, N. Gupta, B. M. Steer, A. J. Ingram, M. Gupta, M. Al-Omran, H. Teoh, P. A. Marsden, and S. Verma. MicroRNA-145 targeted therapy reduces atherosclerosis. *Circulation* 126:S81, 2012.
[63]Maiolino, G., G. Rossitto, P. Caielli, V. Bisogni, G. P. Rossi, and L. A. Calò. The role of oxidized low-density lipoproteins in atherosclerosis: the myths and the facts. *Mediat. Inflamm.* 2013:714653, 2013.
[64]Mckay, C., S. Mckee, N. Mottram, T. Mulholland, S. Wilson, S. Kennedy, and R. Wadsworth. Towards a model of atherosclerosis, 2004. http://www.mathstat.strath.ac.uk/downloads/publications/2005-4atheroreport-2.pdf.
[65]Millon, A., M. Sigovan, L. Boussel, J. L. Mathevet, V. Louzier, C. Paquet, A. Geloen, N. Provost, Z. Majd, D. Patsouris, A. Serusclat, and E. Canet-Soulas. Low WSS induces intimal thickening, while large WSS variation and inflammation induce medial thinning, in an animal model of atherosclerosis. *PLoS ONE* 10:1–14, 2015.
[66]Morton, J., S. Bao, D. Celermajer, M. Ng, and C. Bursill. Striking differences between the atheroprotective effects of high density lipoproteins in early-stage and late-stage atherosclerosis: insights into the lack of efficacy of HDL-raising therapy. *Hear. Lung Circ.* 22:S66–S67, 2013.
[67]Nematollahi, A., E. Shirani, I. Mirzaee, and M. R. Sadeghi. Numerical simulation of LDL particles mass transport in human carotid artery under steady state conditions. *Sci. Iran.* 19:519–524, 2012.
[68]Nematollahi, A., E. Shirani, M. R. Sadeghi, and I. Mirzaee. Effects of shear-dependent transport properties on lumen surface concentration of LDL particles in stenosed carotid artery. *Meccanica* 50:1733–1746, 2015.
[69]Newby, A. C., and A. B. Zaltsman. Fibrous cap formation or destruction—the critical importance of vascular smooth muscle cell proliferation, migration and matrix formation. *Cardiovasc. Res.* 41:345–360, 1999.
[70]Olgac, U., V. Kurtcuoglu, and D. Poulikakos. Computational modeling of coupled blood-wall mass transport of LDL: effects of local wall shear stress. *Am J Physiol Heart Circ Physiol* 294:H909–H919, 2008.
[71]Ougrinovskaia, A., R. S. Thompson, and M. R. Myerscough. An ODE model of early stages of atherosclerosis: mechanisms of the inflammatory response. *Bull. Math. Biol.* 72:1534–1561, 2010.
[72]Panousis, C. G., G. Evans, and S. H. Zuckerman. TGF-beta increases cholesterol efflux and ABC-1 expression in macrophage-derived foam cells: opposing the effects of IFN-gamma. *J. Lipid Res.* 42:856–863, 2001.
[73]Patlak, C. S., D. A. Goldstein, and J. F. Hoffman. The flow of solute and solvent across a two-membrane system. *J. Theor. Biol.* 5:426–442, 1963.
[74]Prosi, M., P. Zunino, K. Perktold, and A. Quarteroni. Mathematical and numerical models for transfer of low-density lipoproteins through the arterial walls: a new methodology for the model set up with applications to the study of disturbed lumenal flow. *J. Biomech.* 38:903–917, 2005.
[75]Rappitsch, G., and K. Perktold. Computer simulation of convective diffusion processes in large arteries. *J. Biomech.* 29:207–215, 1996.
[76]Rappitsch, G., K. Perktold, and E. Pernkopf. Numerical modelling of shear-dependent mass transfer in large arteries. *Int. J. Numer. Methods Fluids* 25:847–857, 1997.
[77]Rayner, K. J., F. J. Sheedy, C. C. Esau, F. N. Hussain, R. E. Temel, S. Parathath, J. M. Van Gils, A. J. Rayner, A. N. Chang, Y. Suarez, C. Fernandez-Hernando, E. A. Fisher, and K. J. Moore. Antagonism of miR-33 in mice promotes reverse cholesterol transport and regression of atherosclerosis. *J. Clin. Invest.* 121:2921–2931, 2011.
[78]Reddy, S., and P. Seshaiyer. Stability analysis of a model of atherosclerotic plaque growth. *Comput. Math. Methods Med.* 1–7:2015, 2015.
[79]Rhodes, J., J. Sharkey, and P. Andrews. Serum IL-8 and MCP-1 concentration do not identify patients with enlarging contusions after traumatic brain injury. *J. Trauma Inj. Infect. Crit. Care* 66:1591–1597, 2009.
[80]Rohatgi, A., A. Khera, J. D. Berry, E. G. Givens, C. R. Ayers, K. E. Wedin, I. J. Neeland, I. S. Yuhanna, D. R. Rader, J. A. de Lemos, and P. W. Shaul. HDL cholesterol efflux capacity and incident cardiovascular events. *N. Engl. J. Med.* 371:2383–2393, 2014.
[81]Sakellarios, A. I., M. I. Papafaklis, P. Siogkas, L. S. Athanasiou, T. P. Exarchos, K. Stefanou, C. V. Bourantas, K. K. Naka, L. K. Michalis, O. Parodi, and D. I. Fotiadis. Patient-specific computational modeling of subendothelial LDL accumulation in a stenosed right coronary artery: effect of hemodynamic and biological factors. *AJP Heart Circ. Physiol.* 304:H1455–H1470, 2013.
[82]Schiopu, A., B. Frendéus, B. Jansson, I. Söderberg, I. Ljungcrantz, Z. Araya, P. K. Shah, R. Carlsson, J. Nilsson, and G. N. Fredrikson. Recombinant antibodies to an oxidized low-density lipoprotein epitope induce rapid Regression of atherosclerosis in Apobec-1-/-/low-density lipoprotein receptor-/- mice. *J. Am. Coll. Cardiol.* 50:2313–2318, 2007.
[83]Schwenke, D., and T. Carew. Initiation of atherosclerotic lesions in cholesterol-fed rabbits. *Atherosclerosis* 9:908–919, 1989.
[84]Seneviratne, A. N., B. Sivagurunathan, and C. Monaco. Toll-like receptors and macrophage activation in atherosclerosis. *Clin. Chim. Acta* 413:3–14, 2012.
[85]Shaaban, A., and A. Duerinckx. Wall shear stress and early atherosclerosis: a review. *AJR Am. J. Roentgenol.* 174:1657–1665, 2000.
[86]Shaw, J. A., A. Bobik, A. Murphy, P. Kanellakis, P. Blombery, N. Mukhamedova, K. Woollard, S. Lyon, D. Sviridov, and A. M. Dart. Infusion of reconstituted high-density lipoprotein leads to acute changes in human atherosclerotic plaque. *Circ. Res.* 103:1084–1091, 2008.
[87]Shu, L., X. Liu, Y. Li, B. Yang, S. Huang, Y. Lin, and S. Jin. Modified Kedem-Katchalsky equations for osmosis through nano-pore. *Desalination* 399:47–52, 2016.
[88]Silence, J., D. Collen, and H. R. Lijnen. Reduced atherosclerotic plaque but enhanced aneurysm formation in mice with inactivation of the tissue inhibitor of metalloproteinase-1 (TIMP-1) gene. *Circ. Res.* 90:897–903, 2002.
[89]Silva, T., A. Sequeira, R. Santos, and J. Tiago. Mathematical modeling of atherosclerotic plaque formation coupled with a non-Newtonian model of blood flow. *Conf. Pap. Math.* 1–14:2013, 2013.
[90]Siogkas, P., A. Sakellarios, T. P. Exarchos, L. Athanasiou, E. Karvounis, K. Stefanou, E. Fotiou, D. I. Fotiadis, K. K. Naka, L. K. Michalis, N. Filipovic, and O. Parodi.

Multiscale—patient-specific artery and atherogenesis models. *IEEE Trans. Biomed. Eng.* 58:3464–3468, 2011.
[91]Skiadopoulos, A., P. Neofytou, and C. Housiadas. Comparison of blood rheological models in patient specific cardiovascular system simulations. *J. Hydrodyn.* 29:293–304, 2017.
[92]Stadius, M. L., R. Rowan, J. F. Fleischhauer, R. Kernoff, M. Billingham, and A. M. Gown. Time course and cellular characteristics of the iliac artery response to acute balloon injury: an angiographic, morphometric, and immunocytochemical analysis in the cholesterol-fed New Zealand white rabbit. *Arterioscler. Thromb. Vasc. Biol.* 12:1267–1273, 1992.
[93]Stanbro, W. D. Modeling the interaction of peroxynitrite with low-density lipoproteins. II: reaction/diffusion model of peroxynitrite in low-density lipoprotein particles. *J. Theor. Biol.* 205:465–471, 2000.
[94]Stangeby, D. K., and C. R. Ethier. Coupled computational analysis of arterial LDLtransport—effects of hypertension. *Comput. Methods Biomech. Biomed. Engin.* 5:233–241, 2002.
[95]Stone, P. H., C. M. Gibson, R. C. Pasternak, K. Mcmanus, L. Diaz, T. Boucher, R. Spears, T. Sandor, B. Rosner, and F. M. Sacks. Natural history of coronary atherosclerosis using quantitative angiography in men, and implications for clinical trial of coronary regression. *Am. J. Cardiol.* 71:766–772, 1993.
[96]Sun, N., N. B. Wood, A. D. Hughes, S. A. M. Thom, and X. Y. Xu. Fluid-wall modelling of mass transfer in an axisymmetric Stenosis: effects of shear-dependent transport properties. *Ann. Biomed. Eng.* 34:1119–1128, 2006.
[97]Tardy, C., M. Goffinet, N. Boubekeur, R. Ackermann, G. Sy, A. Bluteau, G. Cholez, C. Keyserling, N. Lalwani, J. F. Paolini, J. L. Dasseux, R. Barbaras, and R. Baron. CER-001, a HDL-mimetic, stimulates the reverse lipid transport and atherosclerosis regression in high cholesterol diet-fed LDL-receptor deficient mice. *Atherosclerosis* 232:110–118, 2014.
[98]Tedgui, A., and M. J. Lever. Filtration through damaged and undamaged rabbit thoracic aorta. *Am. J. Physiol.* 247:H784–H791, 1984.
[99]Tomaso, G., V. Daz-Zuccarini, and C. Pichardo-Almarza. A multiscale model of atherosclerotic plaque formation at its early stage. *IEEE Trans. Biomed. Eng.* 58:3460–3463, 2011.
[100]Tomaso, G., C. Pichardo-Almarza, O. Agu, and V. Díaz-Zuccarini. A multiscale and patient-specific computational framework of atherosclerosis formation and progression: a case study in the aorta and peripheral arteries. *Proc. Comput. Sci.* 51:1118–1127, 2015.
[101]Vafai, K., and C. L. Tien. Boundary and inertia effects on flow and heat transfer in porous media. *Int. J. Heat Mass Transf.* 24:195–203, 1981.
[102]Wang, S., and K. Vafai. Analysis of low density lipoprotein (LDL) transport within a curved artery. *Ann. Biomed. Eng.* 43:1571–1584, 2015.
[103]Wu, M.-Y., C.-J. Li, M.-F. Hou, and P.-Y. Chu. New insights into the role of inflammation in the pathogenesis of atherosclerosis. *Int. J. Mol. Sci.* 18:2034, 2017.
[104]Yang, N., and K. Vafai. Modeling of low-density lipoprotein (LDL) transport in the artery-effects of hypertension. *Int. J. Heat Mass Transf.* 49:850–867, 2006.
[105]Yang, N., and K. Vafai. Low-density lipoprotein (LDL) transport in an artery—a simplified analytical solution. *Int. J. Heat Mass Transf.* 51:497–505, 2008.
[106]Yang, Y., W. Jäger, M. Neuss-Radu, and T. Richter. Mathematical modeling and simulation of the evolution of plaques in blood vessels. *J. Math. Biol.* 72:973–996, 2016.
[107]Zahedmanesh, H., H. Van Oosterwyck, and C. Lally. A multi-scale mechanobiological model of in-stent restenosis: deciphering the role of matrix metalloproteinase and extracellular matrix changes. *Comput. Methods Biomech. Biomed. Engin.* 17:813–828, 2014.
[108]Zhang, S., L. R. Ritter, and A. I. Ibragimov. Foam cell formation in atherosclerosis: HDL and macrophage reverse cholesterol transport. *Discret. Contin. Dyn. Syst. Ser.* 2013. https://doi.org/10.3934/proc.2013.2013.825.
[109]Zhao, W., C. A. Oskeritzian, A. L. Pozez, and L. B. Schwartz. Cytokine production by skin-derived mast cells: endogenous proteases are responsible for degradation of cytokines. *J. Immunol.* 175:2635–2642, 2005.
[110]Zheng, K. H., F. M. van der Valk, L. P. Smits, M. Sandberg, J. L. Dasseux, R. Baron, R. Barbaras, C. Keyserling, B. F. Coolen, A. J. Nederveen, H. J. Verberne, T. E. Nell, D. J. Vugts, R. Duivenvoorden, Z. A. Fayad, W. J. M. Mulder, G. A. M. S. van Dongen, and E. S. G. Stroes. HDL mimetic CER-001 targets atherosclerotic plaques in patients. *Atherosclerosis* 251:381–388, 2016.
[111]Zohdi, T. I. A simple model for shear stress mediated lumen reduction in blood vessels. *Biomech. Model. Mechanobiol.* 4:57–61, 2005.
[112]Zohdi, T. I., G. A. Holzapfel, and S. A. Berger. A phenomenological model for atherosclerotic plaque growth and rupture. *J. Theor. Biol.* 227:437–443, 2004.